FERMILAB-Proposal-0665

MUON SCATTERING WITH HADRON DETECTION AT THE TEVATRON

a proposal to

FERMILAB

by

F.J.Hazert, D.Lanske, K.Schultze
Physics Institute der Tech. Hochschule, Aachen, F.R.G.

H.G.E.Kobrak, R.A.Swanson
University of California-San Diego, LaJolla, California 92093

R.W.Dobinson, H.E.Montgomery, A.M.Osborne
CERN, Geneva, Switzerland

J.E.Elias, W.R.Francis*, T.B.W.Kirk, J.Morfin
Fermi National Accelerator Laboratory, Batavia, Illinois 60510

W.Mohr, K.Rith, H.E.Stier
University of Freiburg, Freiburg, F.R.G.

G.W.Brandenburg, F.M.Pipkin, R.Wilson
Harvard University, Cambridge, Massachusetts 02139

W.Busza
Massachusetts Institute of Technology, Cambridge, Massachusetts 20139

V.Eckardt, E.Derado, T.H.Kahl, A.Manz, N.Schmitz, G.Wolf
Max Planck Institute for Physics and Astrophysics, Munich, F.R.G.

F.Grard, R.Windmolders
University de l'Etat des Sciences, Mons, Belgium

R.Clifft, P.R.Norton, J.C.Thompson
Rutherford Laboratory, Chilton, Didcot, England

T.H.Burnett, H.J.Lubatti, K.Moriyasu
University of Washington, Seattle, Washington 98195

G.Braun, H.Wahlen
University of Wuppertal, Wuppertal, F.R.G.

*Visiting Scientist

U.S.Spokesman

Thomas B.W.Kirk
FERMILAB
P.O.Box 500-MS 220
Batavia, Il. 60510 USA
Telephone: (312) 840-3683

European Spokesman

Volker Eckardt
CERN
EP Division
Geneva, Switzerland
Telephone: 41-22-83-6111

53 pages

TABLE OF CONTENTS

Introduction 1

Physics Motivation 3

Apparatus 11

Trigger, Acceptance, Resolution and Yields 16

Schedule and Costs 21

References

Figures

Appendix A Muon Trigger Hardware

Appendix B Trigger Logic

Appendix C Dipole Magnet Focussing

INTRODUCTION

The planned 750 GeV high yield Tevatron muon beam will allow an extension to higher energies of the muon scattering program begun at Fermilab and continuing now on the CERN SPS to 280 GeV [1]. We believe that this substantial gain in primary energy will allow further significant steps to be made in at least two important areas of current investigation. These are, first, the study of muoproduced hadrons where the increase in available CM energy W^2 from 500 to 1300 GeV^2 will be important as indicated already from present data. Second, from the study of nucleon structure functions, many detailed questions will remain to be answered for which the gain in primary energy will be crucial in extending the Q^2 domain beyond which heavy flavour thresholds, mass terms and other non-perturbative effects can contribute.

Given these priorities and existence of the new muon beam, it is our view that an open geometry spectrometer will enable exploitation of the largest range of interesting muon physics that can be encompassed in a single experimental setup. Our collaboration proposes to combine two large magnets, the EMC Vertex Magnet and the Chicago Cyclotron Magnet in a spectrometer that will be as powerful as any known. We will use this spectrometer in two basic and for the most part complementary ways to explore:

i) the properties of hadrons recoiling from deep inelastic muon collisions in hydrogen and heavy nucleii. It will be possible to study single quark fragmentation and jet physics in the same CM energy region as e^+e^- annihilation experiments at PETRA where gluon radiation has been observed directly. However, in our case fragmentation of the current and diquark jets(not seen in e^+e^-) can be measured with precise knowledge of the exchanged virtual photon direction.

This physics could in principle be investigated in deep inelastic neutrino scattering and in hard hadron-hadron collisions. In practice, the mean energies of neutrino beams available at the Tevatron into a bubble chamber(the only comparable detector) are lower by nearly an order of magnitude. Figure 1 shows the number of events in our experiment as a function of W^2 from a 1m H_2 target and $3.2 \times 10^{12} \mu^+$s at 750 GeV. The corresponding numbers for the Tevatron ν beam using the same flux of 10^{18} protons are included showing their relatively

limited range in W^2. The study of jets in hard hadron collisions is confused at present energies and transverse momenta. It is much more likely that quark and gluon fragmentation functions as measured in leptoproduction and $e^+ e^-$ annihilation will be used to understand these collisions than the other way around.

ii) Complementing the fragmentation studies that we will pursue in hydrogen and heavy nuclear targets will be the study of nucleon structure functions with these same targets. Although the targets are relatively thin, the event yields for structure function studies are respectable up to Q^2 of 100. In particular, the accessible range of Q^2 increases linearly with primary muon energy at small $x_{BJ}(<0.02)$. This region is of great interest in the study of the Q^2 evolution of sea quark structure functions, Here, all experiments are limited by kinematics rather than rates, which means that the Q^2 range is automatically increased by at least a factor of two beyond that presently available.

We may later wish to extend the structure function measurements to larger Q^2 values by means of long hydrogen/deuterium targets located in the place of the streamer chamber. The present proposal, however, will concentrate on recoil hadron studies and the structure function information that can be obtained simultaneously from our thin targets.

The future committments of collaboration members, particularly those from the EMC working with the vertex spectrometer itself, seem to mesh well with the Tevatron schedule. Specifically, present plans for the muon beam development will allow some essential preliminary studies of the performance and trigger rates in the forward muon spectrometer whilst the EMC vertex spectrometer can remain at CERN until the end of 1984.

The items mentioned briefly in this introduction are elaborated in the following sections of the proposal together with a description of the apparatus, preliminary cost estimates and schedules.

PHYSICS MOTIVATION

As noted briefly in the introduction, we are proposing to investigate two basic physics questions by means of our proposed experiment: i) how the quarks inside a nucleon(or nucleus) are initially distributed in momentum as a function of Q^2 when struck by a virtual photon(tests of QCD applied to nucleon structure functions); ii) how the struck quark propagates in nuclear matter after the collision and fragments into hadrons(QCD, generalized vector dominance, shadowing, etc. studies and tests).

i) Quark and Gluon Jets

It is well known that the current theory of perturbative QCD makes clear predictions concerning the energy and momentum distributions of hadrons produced in lepton-nucleon scattering. In particular, the zeroth order two jet picture from the current quark and diquark fragmentation into hadrons, will be modified by hard gluon radiation(g) from the current quark, producing an additional hadron jet(Figure 2). Such three jet structures have been observed in e^+e^- experiments[2]. In lepton-hadron interactions, the search for perturbative QCD effects mainly has been limited to the behaviour of single hadron inclusive distributions in Z and $p_\perp^2$(Figure 3) with respect to the current jet axis.[3] These distributions give results at large $p_\perp$[4] which are consistent with QCD predictions[5]. However, for the W ranges presently accessible the number of three jet events is small. Indeed it may be only because the lepton experiments have a well defined current direction that one can see these gluon effects at values of W < 17 GeV, whereas the PETRA data seem to give the best evidence for jet broadening for $\sqrt{s}$ > 27 GeV (Figure 4).

The large W^2 region available to this experiment(see Figure 1) and the ability to measure the individual hadrons(streamer chamber and forward spectrometer) will allow us to study the angular energy flow in the centre of mass where one expects to find a broadening of the energy-flow pattern in the forward direction with increasing W(or Q^2). This forward-backward asymmetry can be predicted by QCD. In this case the QCD predictions are exceptionally 'clean' since the angular energy flow integrates over the structure function and at large centre of mass angles is insensitive to the primordial momentum distribution of the partons[6].

ii) Multiplicities and Fragmentation Functions

At present energies, published data from μp and νp experiments show

charged multiplicities $\langle n_{ch} \rangle$ increasing as $\ln W^2$ in approximate agreement with e^+e^- annihilation in the same W range. It is known that the dramatic rise of $\langle n_{ch} \rangle$ in the latter experiments at higher W is associated with a rise in the rapidity plateau near $y = 0$, indicative of gluon fragmentation. In this proposed experiment, the total length of the rapidity extends to 7 units. This will facilitate a cleaner separation of the target and current fragmentation regions, leading to better measurements of the diquark fragmentation function. The function may remain unmodified by pertubative QCD effects. The observation of protons(and antiprotons) at PETRA[7] has aroused interest since it cannot be explained by conventional quark fragmentation models. It will be important to search for these particles in the current jet region in our experiment over a wide range of W and Q^2. Also, higher energies will clarify the determination of the light and heavy quark fragmentation functions enabling the QCD predictions to be tested to higher Q^2. Here it is essential to have good particle identification over a wide momentum range. Finally, the possibility of measuring the gluon fragmentation functions[9] is considerably enhanced.

iii) Charged and Baryon Number for Recoil Hadrons

In addition to the consideration of purely kinematic properties of recoil hadrons without regard to their type, interesting questions can be addressed when th electric charge and particle type is also measured. The so-called leading charge effect is well known; it is presumably an indication of the u or d character of the forward quark. In e or μ hadron scattering, it is positive due to the larger charge of the u-quark and its predominance in protons. It has been speculated that the average charge of the forward jet would be related to the struck quark charge both in e, μ or neutrino events[10]. Experimental measurements, if extrapolated to infinite W, are in agreement with this expectation[11], but in all cases the charge was measured by looking at hadrons of all types. The yields for mesons alone are shown in Figure 5 from an experiment which separated mesons from protons[8]. The net charge carried by the meson cloud for $x_F >$ is ~ 0.2. If one looks at all hadrons with apparent $x_F > 0$, the net charge increases to ~ 0.6. The discrepancy is accounted for by protons with $x_F \gtrsim 0$, whose calculated x_F when treated as π-mesons is positive.

Two experiments[12] have investigated the distribution of residual protons in e-proton scattering; this is defined as the yield of protons minus anti-

protons and thus indicates the distribution of the baryonic charge. These experiments suggest that there are two groupings of protons: one with x_F near -1.0 and the other with $x_F \approx -0.2$(see Figure 6). The relative yield of the latter increases with x_{Bj}, suggesting that it might be connected with interactions involving valence quarks. It is these protons which contaminate the π^+ meson cloud in the forward direction. It also appears that $\bar{x}_F$ for these protons increases with energy.

In order to investigate these phenomena further it is necessary to have a muon spectrometer plus a vertex detector with full x_F and ϕ acceptance. It is also important for the device to be able to separate low momentum pions and protons. These requirements are well matched to our proposed detector.

iv) Hadron Production from Heavy Nucleii

One of the central problems in the quark model of hadron structure is why a quark, when struck by a lepton or some current, is not seen to emerge as a free particle. If the quarks are confined to within the hadron the question then centers upon the dynamics of the confinement process and the closely associated question of the evolution of multiparticle states after the excitation of quarks in an elementary particle collision.

An important technique that is available for directly observing the development of the final states is the use of collisions on nuclei. The idea behind this technique is straightforward: in order to directly study the evolution of a state it is necessary to interfere with it while it is evolving. The distances involved in particle production at high energies are such that nucleus can effectively play the role of the production target followed by an 'interfering system'.

The study of hadron-nucleus collisions has already given a number of surprises and considerable insight into the space-time development of the production process[13]. Unfortunately, because of the compound nature of the incident state and therefore inherent complexity of the initial interaction, a detailed interpretation of the data is difficult. On the other hand, there is good reason to believe that the interpretation of deep inelastic, lepton-nucleus collisions is more straightforward and as a consequence that such studies will give invaluable information on the dynamics of quark fragmentation into hadrons[14].

From a naive quark-parton viewpoint the picture of inelastic lepton scattering of nucleons can be described as follows[15]. A virtual photon is emitted by the lepton in its passage through or near a nucleon. For small values of Bjorken x ($\lesssim 0.1$), the photon has time to produce virtual $q\bar{q}$ pairs before interacting with the nucleon. The photon's interaction is thus hadron-like. For larger x the photon is absorbed by a constituent quark in the nucleon. The struck quark receives an energy ν and attempts to leave the nucleon, but because of the confining forces, it fragments instead into a jet of particles. This fragmentation process takes place over a distance of the order of ν/m^2, where $m \approx 2$ GeV. The range of ν in this experiment extends up to 700 GeV compared with 250 GeV at the CERN SPS.

An alternative viewpoint is that Q^2 and not x is the relevant parameter for separating the hadron-like and point-like regions of the virtual photon[16] In this case, the virtual photon interaction with a quark can be considered point-like for $Q^2 \gtrsim 1$ GeV^2. Our experiment will determine whether crossing a Q^2 threshold is a sufficient condition for observing the effects of individual quarks.

In either case, the scattered lepton effectively tags the hadron jet which is produced in, and passes through, the nuclear matter. For low values of x, or Q^2, the A-dependence of the produced hadrons should be similar to that in hadron-nucleus collisions at an incident energy of ν GeV. This will be an interesting check on our understanding of the process taking place but will probably not contain information which cannot be obtained from hadron-nucleus collisions. However, in the region of pointlike scattering, the variation with ν of the A-dependence of the produced particles should prove fascinating.

Figure 7 summarizes the relation between x, ν, and Q^2 and the various distances of interest in this experiment. The important measurements to be made in such an experiment and their interpretation are as follows:

1) The variation with A of the multiplicity and of the longitudinal rapidity distribution in the direction of the virtual photon gives information on the time structure of the quark hadronization process.
2) A measurement of the attenuation of the leading hadrons as a function of nuclear thickness gives information on the

absorption of fast quarks by nucleons. Furthermore, the difference between π and K attenuation is related to the difference between the absorption cross sections of strange and non-strange quarks.

3) For similar reasons, the A-dependence of the width of the $P_\perp$ distribution of leading hadrons about the direction of the virtual photon gives information on the differential cross section of quarks on nucleons.

Several authors have made predictions of what one might expect to see. Their models for quark fragmentation estimate that hadrons of energy E are formed after a time E/m, where m is of order 2 GeV^2. Thus the multiplicity of high energy hadrons should be independent of the nuclear mass number A except for secondary interactions of the emerging quark. Bialas and Bialas[17] have made estimates for two observable effects of such interactions. The first is a depletion of high energy hadrons as A increases because of inelastic interactions of the quark. Figure 8 shows the expected depletion as a function of A for reasonable choices of the quark-nucleon absorption cross section. The quantity R is the ratio of hadron multiplicity with a nuclear target to that with a hydrogen target. The second effect is a broadening of the distribution $dN/dP_\perp^2$ of high energy hadrons due to multiple elastic scattering of the emerging quark. Figure 9 shows the results of the Bialas model.

Hadrons of low energy and short formation times are produced inside the nucleus and undergo nuclear cascading; this has the effect of depleting the spectrum for high energies and enhancing the multiplicity of low energies. Hadrons formed outside the nucleus do not contribute to this process; the result is a drop in multiplicity with increasing hadron energy which is clearly seen in the calculation of Dividenko and Nikolaev[18] shown in Figure 10. Here R is plotted as a function of hadron momentum k. The interpretation of these curves is relatively straightforward. The highest momentum hadrons are formed outside the nucleus. Their multiplicity is independent of nuclear size, and the threshold k_T, above which R = 1, increases linearly with nuclear radius, but does not depend on quark energy. Hadrons with momentum k just below k_T, are depleted by nuclear cascading; this produces a dip in R around 8-30 GeV/c and an increase in R below 5 GeV/c from the cascade products. This dip is characteristic of the class of models using short range correlation. Models emphasizing the production of hadrons through colour neutralization, as

advocated by Brodsky[16], predict instead that R smoothly interpolates between the target and beam fragmentation regions. We should be able to resolve this issue, hopefully gaining insight into the quark fragmentation process and the interaction of quarks with nuclear matter.

The only published experiment with electrons or muons related to this subject has been done at SLAC at 20 GeV[19] where the formation time was probably too small so that hadron-nucleon scattering dominated the results. The EMC have taken some data at CERN at 200 and 240 GeV on Copper and Carbon targets using their forward spectrometer only. This study will be continued with the new vertex spectrometer and should be a useful first step to a continued program at Fermilab.

v. Inclusive Muon Scattering and Nucleon Structure Functions

Tevatron energy muon beams may be the best means by which the nucleon structure functions can be determined and as a result may be one of the few reliable testing grounds for the preditions of QCD. Figures 11a,b, illustrate the essential character of the QCD predictions for scale violation in the nucleon structure functions as Q^2 is increased. The second order QCD corrections have now been calculated[20] and are explicitly shown in the figures. Since the second order corrections are small, it is likely that the perturbative QCD prediction is reliable and, therefore, legitimates tests of the theory can be made in this area. On the other hand, the small absolute magnitudes of the QCD scale violating effects and their slow Q^2 variation will continue to present a formidable challenge to experimenters who want to move beyond the results achieved to date.

At first sight, it appeared that the most critical tests of perturbative QCD to leading order could be made in the comparatively low Q^2 region. This was the prevailing view in analyses of the data from earlier electron, muon and neutrino experiments where comparison with QCD predictions appeared satisfactory[21]. However, it was demonstrated that i) general features of scale violations could be obtained by many field theory models[22] not only QCD, and ii) second order QCD calculations were done and other higher order effects[23] estimated which cast doubt on the earlier conclusions. In particular, the so-called 'higher twist' effects[24] seem to put a lower limit on the Q^2 range where reliable comparisons can be made between QCD and experimental results. Given these above complications, it is clear that measurements ought to extend to $Q^2 \gtrsim 20\ (\mathrm{GeV/c})^2$ at all values of x_{Bj} for comparison with theory.

However, here again there is a problem. Even if extreme centre of mass collision energies are possible(ep colliders), two things conspire to limit the power of a QCD test: i) the integrated number of events, hence the statistical power of the test, drops as $1/Q^2$, making luminosity requirements more severe as the Q^2 scale rises; ii) the ordinary QED radiative corrections can become extremely large for ep collider energies. While calculable in principle, these large corrections must influence the reliability of observing the much smaller QCD effects on is attempting to measure.

With Tevatron energy muon beams, the useful Q^2 range experimentally accessible is broad enough to investigate these QCD effects, and radiative corrections are reliable and small. However, we are faced with the question of target and method. The natural targets are hydrogen and deuterium, but to reach very high values of Q^2 it will be necessary to use long targets(tens of metres). If such targets are used, vertex location, hence Q^2 resolution, may be compromised resulting in unacceptable systematic errors at low values of Q^2. We propose a solution to these problems in the section on resolutions and yields.

As noted in the introduction, the beam energy gain made at the Tevatron gives us a special advantage for the small and wee x_{Bj} region. In this regime, the linear gain with beam energy with Q^2 at a fixed value of x_{Bj} means that the properties of ocean quarks can be investigated with much less worry about domination by non-perturbative effects. From Figures 17 and 18 we see, for example, that there are thousands of events for which $0.01 \leqslant x_{Bj} \leqslant 0.10$ all of which have $Q^2>5(\mathrm{GeV}/c)^2$. This is a very interesting region which cannot be investigated by bubble chambers using neutrino probes. This field will be dominated by open geometry muon spectrometers until the eventual appearance of ep collider spectrometers.

APPARATUS

The spectrometer as we currently imagine it is shown in Figures 12 and 13. As noted before, it is based on two large superconducting dipole magnets instrumented to measure essentially all recoil particles above 200 MeV/c momentum. The upstream magnet and detectors consist of the transplanted EMC Vertex Spectrometer; the downstream magnet is the CCM outfitted with superconducting coils. Instrumentation of the downstream magnet and subsequent detectors consists partly of existing detector systems and partly of new or upgraded ones. We discuss the elements of the spectrometer and its capabilities here in some detail.

i) Vertex Magnet and Streamer Chamber

The EMC vertex system is shown in Figure 12. It consists of a streamer chamber inside a superconducting magnet with additional external detectors to aid track reconstruction accuracy and identify particles out to large angles.

The vertex magnet is a dipole type superconducting magnet with circular coils of 2m inner diameter and a separation of 1m. The maximum field is 1.5T. The large aperture in the forward direction allows particles produced within $\pm 60^0$ in the horizontal plan and $\pm 10^0$ in the vertical plane to leave the magnet. The 2m diameter hole in the pole permits optical recording parallel to the magnetic field for highest possible accuracy.

The streamer chamber has dimensions 2m x 1.2m x 0.72m. The depth of 0.72m is subdivided into three gaps 2 x 18cm and 1 x 36cm in the centre. A 1m long liquid H_2 target with a 70mm diameter target cell and 118mm outer diameter is located in the upstream part of the sensitive volume. The HV power supplies feeding the Marx generator and the film velocity of the camera equipped with image intensifiers allows a repetition rate of 5 pictures/sec as presently used in the CERN NA5 experiment. Recent tests have shown that beam intensities up to 10^7/sec can be handled without precaution against δ-electrons.

ii) Vertex Magnet Associated Detectors

To reduce the matching problems between the streamer chamber and the external detectors, MWPC's(PV1,2,3) are placed at the end of the streamer chamber body still inside the magnet. Large area TOF hodoscopes(F1,2,3,4), drift tube planes(WV1,2,3) and small MWPC's are used for track measurements serving as a lever arm for momentum determination. In the central region up

to a scattering angle of 10^0, two large multicell Cerenkov counters(CØ, C1) achieve good π/K and p separation from 2.5 GeV/c. The counter CØ extends into the large angle region and is supplemented by a large aerogel system (CA) and the TOF hodoscopes. In this angular region there is good π/K separation up to 9 GeV/c, and $\pi/K/p$ separation to 5 GeV/c.

To assess the suitability of this system at Tevatron energies, hadron final states have been generated in a Monte Carlo program[25] taking into account QCD graphs up to the 1st order and assuming Feynmann-Field type fragmentation of the jets. The scattered muon and the produced hadrons are then tracked through the vertex system and a forward spectrometer with an acceptance of 2 x $1.2m^2$. Figure 14a shows a 3 jet event at W = 30 GeV, Q^2 = 50 GeV selected by requirement that $p_\perp > 1.22$ GeV/c for at least one charged particle in the hadron CM system. The charged multiplicity in this example is 16 of which only 6 hadrons plus the scattered muon can be fully analysed by the forward spectrometer alone. Figure 14b demonstrates the pattern recognition requirements for the streamer chamber. It should be noted that on average 6 muon beam tracks will be present at a rate of 3 x $10^6 \mu$'s/sec and a memory time of 2.2μ sec in the streamer chamber.

The distribution in momentum and position of charged hadrons in the external detectors has been compared with a 2 jet model at 750 and 280 GeV μ energy. The results are listed in Table 1 and generally show that although there is some reduction(up to a factor of 50%) of particles in the outer region beyond $\pm 10^0$, the momentum distributions there are very similar.

iii) CCM Magnet Associated Detectors

To continue the tracking of charged particles into the CCM and beyond, there are sets of multiwire proportional chambers and drift chambers. As charged particles exit the Vertex Spectrometer and enter the CCM they pass through a set of 10 MWPC planes of active area 80cm x 80cm and wire spacing 1.6mm. These planes constitute the necessary lever arm for momentum measurements on particles in the few GeV range where the Vertex Magnet alone would have less than the desired resolution. They also sort out the orbits of individual particles of tens to hundreds of GeV and whose lever arm is supplied by the drift chambers downstream of that magnet.

Within the aperture of the CCM, there is placed a set of 15 MWPC planes grouped as uyv triplets. The chambers have an active area 1.2m x 1.0m and

TABLE 1

Charged Hadron Distributions

μ interactions in 1m H_2 target

	750 GeV	280 GeV
Charged multiplicity $\langle n_{ch} \rangle$	11	8.3
Mean hadron momentum (GeV)	26	9
Proportion of all hadrons in central PV2	86%	83%
Proportion of all hadrons in outer PV1, 3	4%	5%
Proportion of all hadrons in outer WV1, 2	15%	20%
Proportion of all hadrons in outer TOF	6.5%	9%
Mean momentum through CA, outer CØ (GeV)	2.6	2.6
Mean momentum through C1, central CØ (GeV)	35	14

NB: Conditions - 750 GeV

$250 < \nu < 750$ GeV, $0 < Q^2 < 600$ GeV^2

280 GeV

$0 < \nu < 250$ GeV, $0 < Q^2 < 200$ GeV^2

and a wire spacing of 2.0mm. These chambers add momentum resolution to the measurement of tracks which have less than about 10 GeV and which are largely thrown out of the acceptance of the downstream drift chambers. They also add to the pattern recognition reliability for all orbits passing through the magnet.

Immediately downstream of the magnet is placed a set of four drift planes of active area 2.2M x 1.5M. Each drift plane measures both horizontal and vertical position to yield correlated(x,y) points[26]. The horizontal coordinate is obtained from the drift time in the usual way and has a resolution better than 200μ. The vertical coordinate is measured by time of flight of the induced charge on a printed circuit delay line and has a resolution of about 1 cm.

The vertical coordinate is useful more for the purposes of pattern recognition than for vector momentum reconstruction. The vector momentum reconstruction

depends upon the MWPC's in the CCM(intermediate momenta) and the final drift chamber array(high momenta). The horizontal coordinate, however, is important for determining the orbit deflection through the CCM and hence the momentum of high momentum tracks.

The final set of drift chambers is located behind the multicell threshold Cerenkov counter. It consists of a set of 6 drift planes of active area 7.0M x 3.0M(2 each of y,u, and v coordinates) constituting a shallow angle stereo system for measurement of both horizontal and vertical coordinates. The cell size is 5.0 cm for all coordinates and each drift measurement will have a resolution of 200μ or better. This system will have a total of 840 drift channels. Hoever, it should be noted that the final choice of cell size, exact plane configurations and number will depend on detailed Monte Carlo study.

Of the tracking systems just described, all but the final drift chamber array exist and are being used in Fermilab E610, an experiment now set up around the CCM. The drift chamber electronics for the existing drift chambers is of the low-deadtime, multihit variety and can be used without modification for the new drift chamber module.

iv) Multicell Cerenkov Counter

We propose to extend the radiator length of our existing 18 cell threshold Cerenkov counter to 5m, with suitable modifications for Helium gas and use it for proton separation above the useful range of C1. This counter would then have threshold of 112 GeV, 58 GeV and 17 GeV for protons, kaons and pions, respectively. The photoelectron yield for a practical optics should be about 5 corresponding to a $\beta = 1$ particle. This is adequate for our purposes.

We know from our previous work in the CCM that the granularity of the Cerenkov counter is satisfactory for the expected flux of charged secondaries which can make it through the two magnet deflecting fields. If more exacting studies suggest restructuring of the mirror array, we will have plenty of time to accomplish this work.

v) Beam Tagging and Halo Veto

We will instrument the final bending magnet in the muon line with MWPC chambers and tagging/triggering scintillation hodoscopes to allow electronic definition of clean beam trajectories for the fast trigger and subsequent orbit and momentum reconstruction of accepted events on a one by one basis.

Beam tagging stations will be located at the downstream end of the final FODO quadrupole, at both ends of the tagging dipole, and just upstream of the vertex magnet. Appropriate veto counters will be placed around the tagging dipole to define its aperture electronically. A large veto wall will be erected in front of the vertex magnet. The two veto elements are necessary for the suppression in the fast trigger of halo muons moving through the dirt outside the beam.

The beam tagging and halo suppression techniques are by now well known and we will not elaborate further except to note that they can probably be largely constituted from existing systems at Fermilab with little or no modification.

vi) Muon Detector Array

We plan to use a two plane scintillation counter array of appropriate granularity and overall dimensions 7.9m x 4.4m to trigger on a muon scattered out of the beam. A small counter placed in the unscattered beam will be used to aid in suppression of random conincidence triggers. We haven't decided on the precise counter geometry, but there will be of order 50 counters per plane which will be arranged to allow several levels of prescaling for high rate triggers relative to low rate ones.

In addition to the scintillation counter arrays, there will be a set of 12 proportional tube planes decoupled by concrete walls to allow microprocessor presorting of fast triggers and rejection of patently bad ones on the basis of a proportional tube signature. The tubes will be fabricated from extruded aluminum shapes in a manner already in use by a number of groups at CERN, Fermilab and elsewhere. Each coordinate will have two layers of half overlapped tubes for efficiency. The tube diameter will be 2.5cm. A total of 1400 tubes will be needed, together with appropriate amplifier and read-in electronics.

None of the scintillation counter or proportional tube arrays exist and this system must be newly fabricated.

vii) Computer and Data Acquisition

In view of the fact that the proposed spectrometer splits rather cleanly into two parts, one connected with the vertex spectrometer and the other connected with the CCM, and because the two elements have been developed in Europe and in the U.S., respectively, we will likely use two PDP 11/45

computers for data acquisition and test. Whether one is slaved to the other or two data streams emerge will depend on the technical advantages and the amount of software effort available.

With the hardware and software concentrated in two different machines, it should be possible to accomplish much of the development of the necessary software systems prior to uniting the physical detectors if this proves convenient.

TRIGGER, ACCEPTANCE, RESOLUTION AND YIELDS

i) Trigger

The trigger for the muon experiment is simple and of a conventional fast/slow type. It has as its basic purpose detection of the nuclear interaction of a cleanly defined beam muon with a Q^2 above some minimum value and with a ν in some acceptable energy range. Because the nuclear scattering probability for muons is a steep function of Q^2, a system of prescaling of higher rate triggers will be used to insure a balanced data sample and acceptable live time fractions for the apparatus. Some precaution is taken to suppress false triggers arising from the accidental coincidence of halo muons outside the beam with real beam particles. We outline the basic system here and leave the technical details to Appendices A,B,C.

The fast trigger is given symbolically by:

$$T_i = CB \cdot \overline{VB} \cdot (M1 \cdot M2)_i \cdot \overline{V},$$

where

T_i = ith fast scattered muon trigger, prescaled by an appropriate factor

CB = clean beam muon into target

VB = small beam centered veto downstream of muon trigger planes

V = veto wall to guard against halo muons

M1,M2 = muon scintillation hodoscopes

The scintillators(See Figure 13) which make up planes M1 and M2 are connected to correspond to allowed scattered muon trajectories of various rates. The high rate combinations will be prescaled so that they will not consume large amounts of deadtime resulting in unnecessarily large samples of low ν and low Q^2 events. The high Q^2, low rate triggers are rare and will require no prescaling. The various combinations will be overlapped in such a way as to be self-checking for absolute efficiencies. The beam trigger CB itself will be prescaled by a factor of 10^7 or so in order to generate a beam phase space measurement taken along with the inelastic scattering data. Other specialized triggers will be used for diagnostic purposes, but we will not go into them here.

The fast trigger T_i will cause the data from the muon proportional tube

planes, the various trigger counters and certain other selected data to be read into temporary storage where it will be examined by a microprocessor based fast trigger processor. In times of order 50μs, a decision can be reached to accept the trigger as an event or to reject it, clear the various detector devices and reopen the fast trigger. Hence,

$$E_i = f(T_i, \text{prop. tubes, etc.})$$

where

E_i = acceptable slow event trigger for full data recording

$f(T_i$, prop.tubes, etc.) = microprocessor based pattern recognition in muon spectrometer plus beam detectors.

For accepted events, the data acquisition computer will read in all the data from the apparatus, record appropriate other information, reset the apparatus and reopen the fast trigger for the next event. This should require on the order of a few milliseconds.

The streamer chamber must be triggered by the fast trigger T_i since it has a short memory time of $\sim$ 1-2 μsec. A further selection of good muon scatters will be done using information from the fast trigger processor or off-line from fully reconstructed events in the muon spectrometer.

The trigger elements and associated devices are discussed in more detail in Appendices A and B. The action of the two spectrometer magnets in producing an approximate achromatic focus of equal muon scattering angles is discussed in Appendix C.

We have yet to decide on the exact magnet geometry and field strengths, but the results for acceptance and momentum resolution are only weakly dependent on these details and will have a small effect on the results.

Important here is the fact that the total trigger rate will be custom prescaled to yield a deadtime below 15% and generate a statistically adequate event sample in all but the highest Q^2 regime where the basic cross section limits the yield from a thin target.

ii) Targets and Luminosity

We will divide the proposed program into two Phases. The goal of Phase I will be the study of hadrons produced in muon interactions of low to moderate Q^2 and high ν with hydrogen, deuterium and heavy nuclear targets. The full

two magnet spectrometer system will be used with 600-750 GeV incident muons. The physics goals of this part of the proposal are covered in sections i-iv) of the physics motivation.

Phase II of the program will involve the use of a long(approximately 10M) liquid hydrogen/deuterium target located in place of the streamer chamber in the Vertex Magnet aperture. This arrangement will allow measurement of nucleon structure functions up to Q^2 values of several hundred GeV^2 with high precision and excellent resolution for the testing of second order QCD predictions. For the reasons elaborated in section v) of the physics motivation, we believe that the high resolution capability will be relevant even at a late point in the program, principally because of the difficulty in eliminating subtle systematic errors in the competing methods and the availability of high luminosity targets of hydrogen and deuterium.

The targets for Phase I are shown in Table 2 and the luminosities and muon exposures for both Phases are shown in Table 3. We have not yet decided whether to use solid/liquid targets or high pressure gas targets for the heavy nucleii so both possibilities are shown in Table 2.

iii) Acceptance, Resolution and Yields

The very large aperture of the CCM combined with the very high energies of the Tevatron muon beam allows a very large acceptance for scattered muons, even when the target is placed 10M upstream in the center of the Vertex Magnet. The large value of $\int Bdl$ for the CCM allows good momentum resolution to be maintained at the same time. To take advantage of the large CCM aperture, a 4.4M x 7.0M detection module for scattered muons is placed behind the downstream apparatus(Figure 13). Most of the muons which scatter out of the beam pass through this module. The exceptions are muons from very high y events with large Q^2. To epitomize the dependence of acceptance on the kinematic parameters, we give a particular example appropriate to the Phase I targets in Figure 15. For runs with the 10M liquid target, the acceptance is virtually identical. If lower beam energy runs are attempted later to extract the value of $R = \sigma_o / \sigma_L$, the acceptance is somewhat smaller but still good.

The resolution in muon momentum and scattering angle is presented in Figure 16. The excellent resolution which can be achieved in our apparatus will be crucial to careful tests of QCD in Phase II of the experiment. In

TABLE 2

Targets for Phase I

Name	A	$A^{2/3}$	$A^{1/3}$	t(cm)	t(gm/cm^2)	X_{oEM}	X^+_{oNucl}
LH_2	1.01	1.01	1.00	100	7.1	.11	.086
LD_2	2.01	1.59	1.26	100	16.3	.13	.16
LN_2	14.01	5.81	2.41	10	8.1	.21	.04
Ar§	39.95	11.83	3.38	100	3.6	.18	.05
Xe§	131.30	26.26	5.00	100	11.7	--	.11
CsI*	129.9	25.65	5.06	0.80*	3.6*	.42*	.008

*This target will be in the form of 4 uniformly spaced disks in the first 1M of the streamer chamber sensitive volume.

§Gas target under 20 atm pressure

+We use $\sigma_{inel.}(\pi N) = 20mb$ and $\sigma_{inel.}(\pi A) = A^{2/3}\,\sigma_{inel.}(\pi N)$ to define X_{oNucl}.

TABLE 3

Luminosities for Muon Targets

Phase/Run	Target (gm/cm^2)	N_μ (x 10^{12})	E_μ (GeV)	Beam Hrs. (7 x 10^{12}p/pulse)
I/1	LH_2(7.1)	2.20	600*	1000
I/2	LD_2(16.3)	2.20	600	1000
I/3	LN_2(8.1)	0.66	600	300
I/4	C_sI(3.6)	1.54	600	700
II/1	LH_2(71)	2.20	600	1000
II/2	LD_2(163)	2.20	600	1000

*This energy could be higher in proportion if the Tevatron protons are above 800 GeV.

Phase I, the superior resolution will contribute not only to the precision obtainable for nucleon structure function measurements at low Q^2 and high X_{Bj}, but also to the measurements of charged hadrons and the interpretation of their $P_\perp$ and Z behavior in terms of QCD.

The event yields obtainable with the acceptance of Figure 15 and for the targets of Table 3 are displayed in Figures 17 and 18 for the 1M hydrogen/deuterium and heavy nuclear targets, respectively. The actual event yields will be lower by the chosen prescale factors in the high yield bins below $Q^2 = 2$. Events from the "almost real" Q^2 range between 0.1 and 2.0 will also be taken with appropriate prescale factors to extract the physics of nuclear shadowing and to make contact with experiments using real photons.

TIME SCHEDULE AND COSTS

It is expected that the first muon beam from the Tevatron will be available in 1984. At this time, the CCM forward spectrometer is planned to be ready for studies. The EMC vertex system will be used in an approved program of physics from 1981 until the end of 1984 at CERN. It will then be transported to Fermilab as a working system. To facilitate the installation of the combined spectrometers on a shorter time-scale, it is possible that an identical vertex magnet could be transported to Fermilab beforehand. The presently used EMC Vertex magnet would remain at CERN.

Despite these long time-scales, we would like to receive Stage 1 approval as soon as possible so that we may begin the long range planning and development that is becoming increasingly necessary for the successful carrying out of a major experimental program.

It is also of significant concern that large pieces of equipment are involved(Vertex Spectrometer and CCM) and their efficient exploitation for physics rests in a substantial way on knowing how they will be used over a period of years. Both devices mentioned above are already included in experimental programs for the period of 1981-1983(longer in the case of the Vertex Spectrometer).

The physicists who built and operate the various systems of the spectrometers would also like to know whether they can plan on further exploitation of their several detectors in a productive program of muon physics. If(as often happens) the decision to approve or reject this experiment is delayed, it will become more and more likely that attractive alternative uses for the system components will arise, as will tempting opportunities for the physicists to apply their skills elsewhere. Eventually, what is now a complete and coherent group with a compelling physics objective could become scattered and fragmented, a situation which would undermine the goal of mounting a powerful attack on muon physics with hadron identification as an integral part of the Tevatron program.

We hope these arguments combined with the strong positive recommendations by the Fermilab Physics Advisory Committee for a Tevatron muon beam and muon physics program[27] will result in a prompt decision on Stage I approval for our proposal. If we can supply any further material or answer any specific

questions that will aid in a prompt decision, we stand ready to comply at once.

The costs of bringing this experiment to readiness are known only in a preliminary way at present. Indeed, the purpose of having a staged approval process explicitly recognizes that arriving at a precise cost involves discussions between experimenters and Fermilab and often involves several other funding sources as well. Accepting these vagaries, we follow the traditional practice of estimating costs for supplying new items called for in the proposal, refurbishing or improving existing ones, shipping the Vertex Spectrometer and moving the CCM to the new muon area. This is done in Table 4.

If this sum is compared to the cost of duplicating the existing facilities it looks very attractive, though the dollar amount is perhaps in the high medium range for contemporary experiments. When the cost to physics benefit analysis is done for this proposal, we believe it will compare favorably with others that have been or will be presented to Fermilab.

Table 4

New Costs for this Experiment
(FY80 U.S. dollars)

Item	Cost (thousands)
Ship and Erect Vertex Spectrometer (CERN to Fermilab)	165
Move, Erect and Power Superconducting CCM	300
Muon Scintillation Planes M1, M2	80
Muon Proportional Planes (including read-in system)	90
Trigger Processor	40
4M x 7M Drift Planes (6 including 1700 channel read-in system)	120
Miscellaneous rework, add counters, etc.	80
TOTAL	875

References

1) CERN/SPSC/77-113 (1977),
CERN/SPSC/80-80, Sept. 1980.

2) TASSO Collaboration, Phys. Lett. 86B, 243 (1979),
MARKJ Collaboration, Phys. Rev. Lett. 43, 830 (1979),
PLUTO Collaboration, Phys. Lett. 86B, 418 (1979),
JADE Collaboration, Phys. Lett. 81B, 142 (1980).

3) 'Recent Results on Hadronic Final States in Charged Current Neutrino and Antineutrino Reactions', N. Schmitz, Proceedings of 1979 Int. Symp. on Lepton Interactions at Fermilab, p. 359,
J. Blietschau et al., Phys. Lett. 87B, 281 (1979).

4) EMC, J.J. Aubert et al., CERN-EP/80-119, to be published in Phys. Lett.,
Berkeley/Hawaii/FNAL/Seattle/Wisconsin Collaboration, contribution to the XX Int. Conf. on HEP, Madison 1980,
H. Deden et al., CERN-EP/80-66 (1980),
C. Tao et al., Phys. Rev. Lett. 44, 1726 (1980).

5) G. Altarelli and G. Martinelli, Phys. Lett. 76B, 89 (1978),
F. Halzen and D.M. Scott, DOE-ER/00881-157, Aug. 1980, Univ. of Wisconsin preprint,
and others,

6) F. Halzen and D.M. Scott, ibid.
R.D. Peccei and R. Ruckl, MPI-PAE/PTh 26/80 July 1980, Max-Planck Inst. preprint.

7) TASSO Collaboration, DESY 80/49 (1980).

8) J.F. Martin et al., Phys. Rev. D20, 5 (1979).

9) B. Anderson and G. Gustafson, Z. Physik C3, 223 (1980).

10) R.P. Feynman, Neutrino Conference, Balaton, Hungary (1972).

11) N. Schmitz, Lepton-Photon Conf. Fermilab 1979.

12) C.J. Bebek et al., Phys. Rev. Lett. 34, 1115 (1975),
L.S. Osborne et al., Phys. Rev. Lett. 41, 76 (1978),

13) W. Busza, Acta Phys. Polon. B8, 333 (1977).

14) J.D. Bjorken, Int. Summer Inst. on Theor. Particle Physics, Hamburg 1975.

15) V.N. Gribov, JETP 30, 709 (1970).

16) S.J. Brodsky, Workshop on Ultra-Relativistic Nuclear Collisions, Berkeley 1979.

17) A. Bialas and E. Bialas, Phys. Rev. D21, 625 (1980).

18) G.V. Davidenko and N.N. Nikolaev, Nucl. Phys. B135, 333 (1978).

19) L.S. Osborne et al., Phys. Rev. Lett. 40, 1624 (1978).

20) A. Bialas and A. Buras, Fermilab-Pub-79/73.

21) H.L. Anderson et al., Phys. Rev. Lett. 40, 1061 (1978), J.G.H. de Groot et al., Phys. Lett. 82B, 292 (1979).

22) H. Harari, Nucl. Phys. B161, 55 (1979).

23) W.A. Bardeen et al., Phys. Rev. D18, 3998 (1978).

24) M. Barnett, SLAC-Pub-2396 (1979).

25) Ch. Rumpf and G. Kramer, DESY/79/62.

26) M. Atac and J. Urish, Nucl. Instr. and Methods 156, 163 (1978).

27) Fermilab Report, July 1980.

FIGURE CAPTIONS

Figure 1 Comparison of events generated in an open geometry muon experiment and in a large neutrino bubble chamber for 10^{18} incident Tevatron protons.

Figure 2 Representative diagrams for quark and gluon fragmentation into jets a) 2 jets $q + qq$; b) 3 jets $q + g + qq$; c) 3 jets $q + \bar{q} + qq$.

Figure 3 a) Measurements of $< P_\perp^2 >$ with muons and neutrinos showing the increase with W^2 as a function of Z .
b) $< P_\perp^2 >$ for the same data averaged over Z . The rise is consistent with QCD predictions for gluon radiation.

Figure 4 The distributions in $< P_\perp^2 >$ for narrow and wide $q\bar{q}$ jets as a function of and X_p for two different ranges of s. Data are from TASSO and PLUTO groups, respectively(Ref.2).

Figure 5 The π^+ and π^- meson yields for recoil hadrons in a low energy ep experiment are shown as a function of Z. The leading hadron shows the charge retention characteristic of u quark domination.

Figure 6 Results from the experiments of Reference 12 in which the properties of final state protons(baryons) were studied as functions of s and Q^2. At Tevatron energies, the kinematic regions accessible should clarify the surprising results seen here.

Figure 7 Characteristic time and distance scales for meson formation from quarks struck by virtual photons. The behavior with ν is shown functionally and that with Q^2 is given parametrically.

Figure 8 Nuclear rescattering of struck quarks in the model of Bialas and Bialas(Ref.17) is shown as a depletion with increasing nucleon number A of the high X hadrons. Results are shown for various quark nucleon cross sections.

Figure 9 Broadening of the $P_\perp$ distribution of high X hadrons by nuclear rescattering is shown for various values of nucleon number A in the model of Bialas and Bialas(Ref.17).

Figure 10 Ratio of hadron multiplicity for varying nuclear radius relative to hydrogen as a function of nucleon momentum in the model of

Davidenko and Nikolaev(Ref.18). Note the depletion for high (but not asymptotic) values of ν, and the increase for low momentum hadrons.

Figure 11 QCD predictions in second order for the Q^2 behavior of the nonsinglet structure function is deeply inelastic scattering. The Q^2 dependence is shown for varying X_{Bj}(Ref.20).

Figure 12 EMC Vertex Detector: PV1-3 MWPC's in magnet aperture; F1-F4 TOF Hodoscopes; CØ, C1, CA Cerenkov counters; WV1-2 Drift Tube assemblies; STR Streamer Chamber.

Figure 13 Proposed Tevatron Muon Spectrometer layout showing Vertex Spectrometer and CCM Spectrometer elements combined into a single integrated detector.

Figure 14 Computer reconstruction of a muon event in the spectrometer a), and the streamer chamber b). The event details are given in the text.

Figure 15 Event acceptance for the spectrometer of Figure 13. The acceptance shown is geometrical only and does not include the effects of electronic prescaling of the low Q^2 trigger.

Figure 16 Resolution in $Y = \nu/E$ and Q^2 for the proposed spectrometer (Figure 13). The y resolution is independent of Q^2.

Figure 17 Event yields for the proposed spectrometer with LH_2 and LD_2 targets including the effects of geometrical acceptance, but not including the electronic prescaling for low Q^2 events.

Figure 18 Event yields for two possible heavy nuclear targets. Geometrical acceptance is shown, but the electronic prescaling cut is not shown.

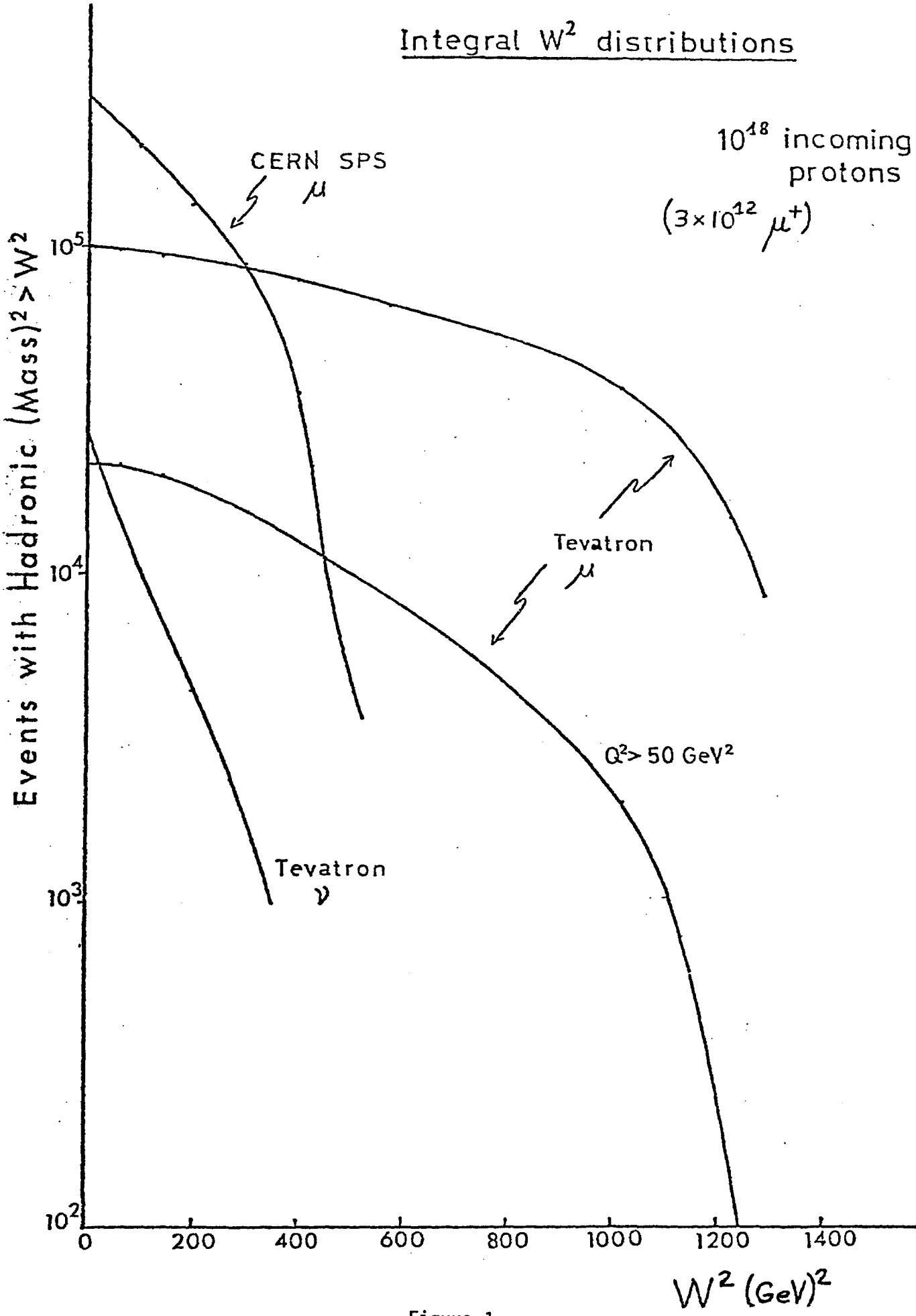
Integral W² distributions
10¹⁸ incoming protons
(3×10¹² μ⁺)
CERN SPS
μ
Tevatron
μ
Tevatron
ν
Q²> 50 GeV²
Events with Hadronic (Mass)² > W²
10⁵
10⁴
10³
10²
0
200
400
600
800
1000
1200
1400
W² (GeV)²

Figure 1

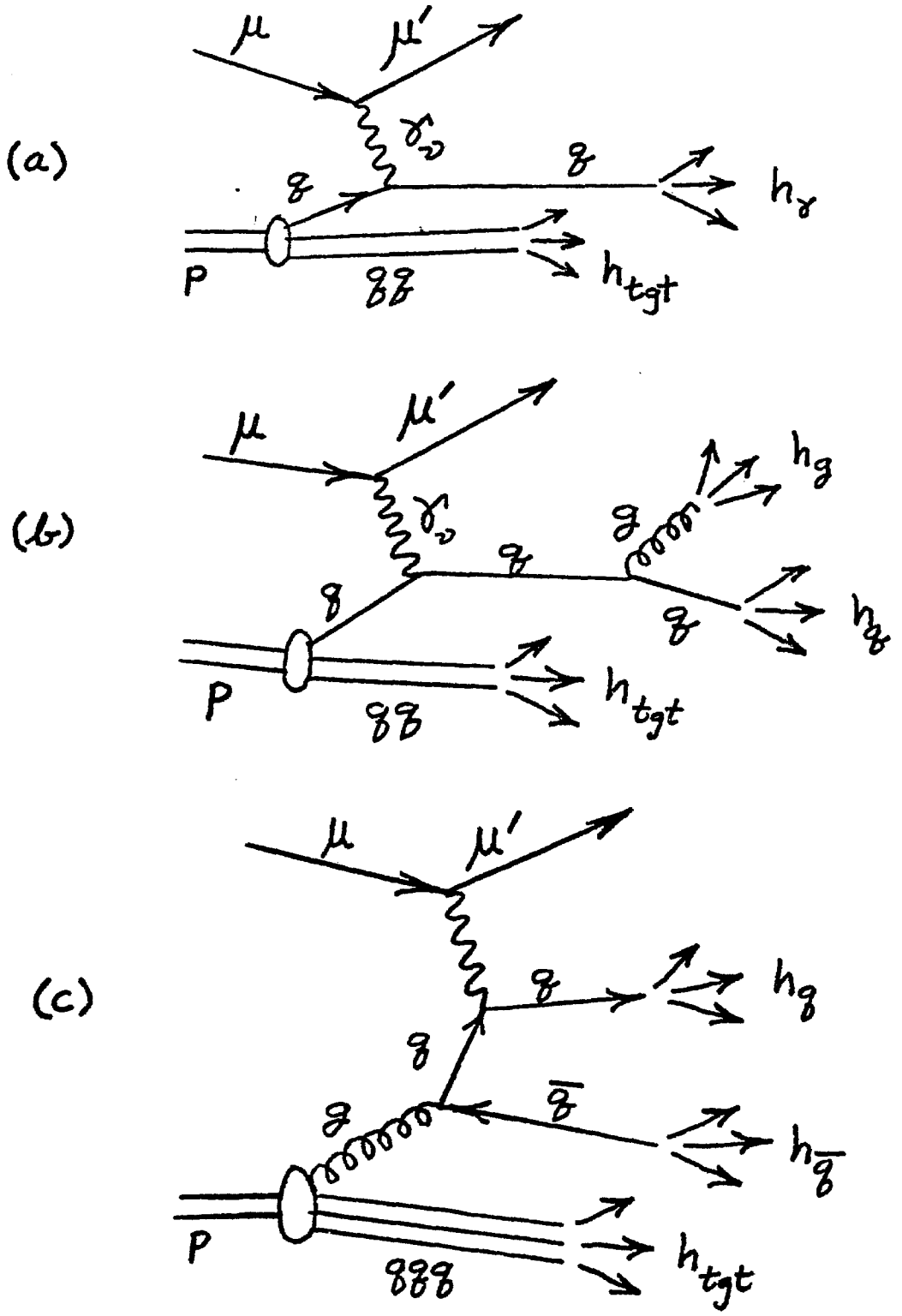
(a)
μ
μ′
γ
q
q
h_γ
P
qq
h_tgt
(b)
μ
μ′
γ
q
g
h_g
q
q
h_q
P
qq
h_tgt
(c)
μ
μ′
q
h_q
q
q̄
g
h_q̄
P
qqq
h_tgt

Figure 2

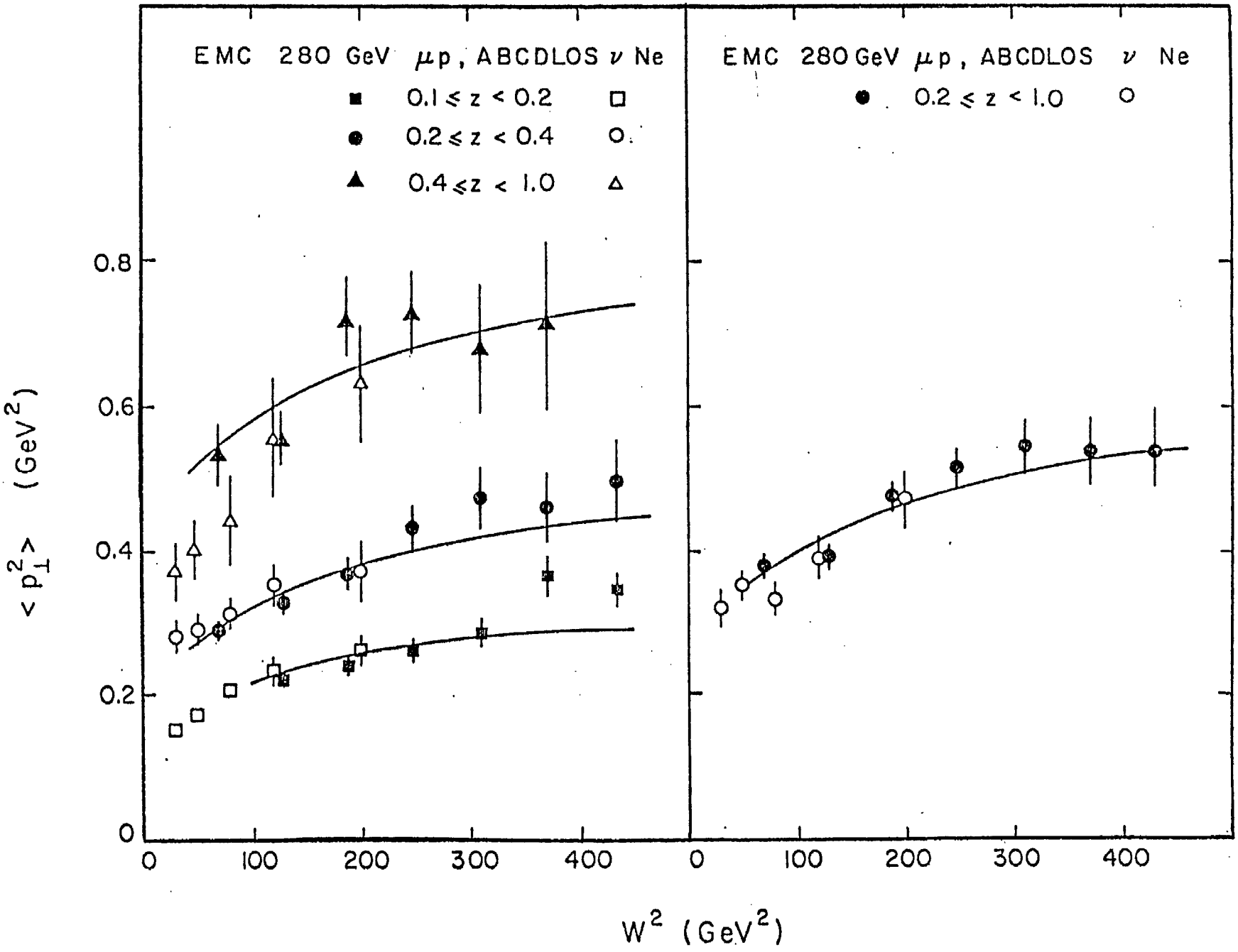

Figure 3a

Figure 3b

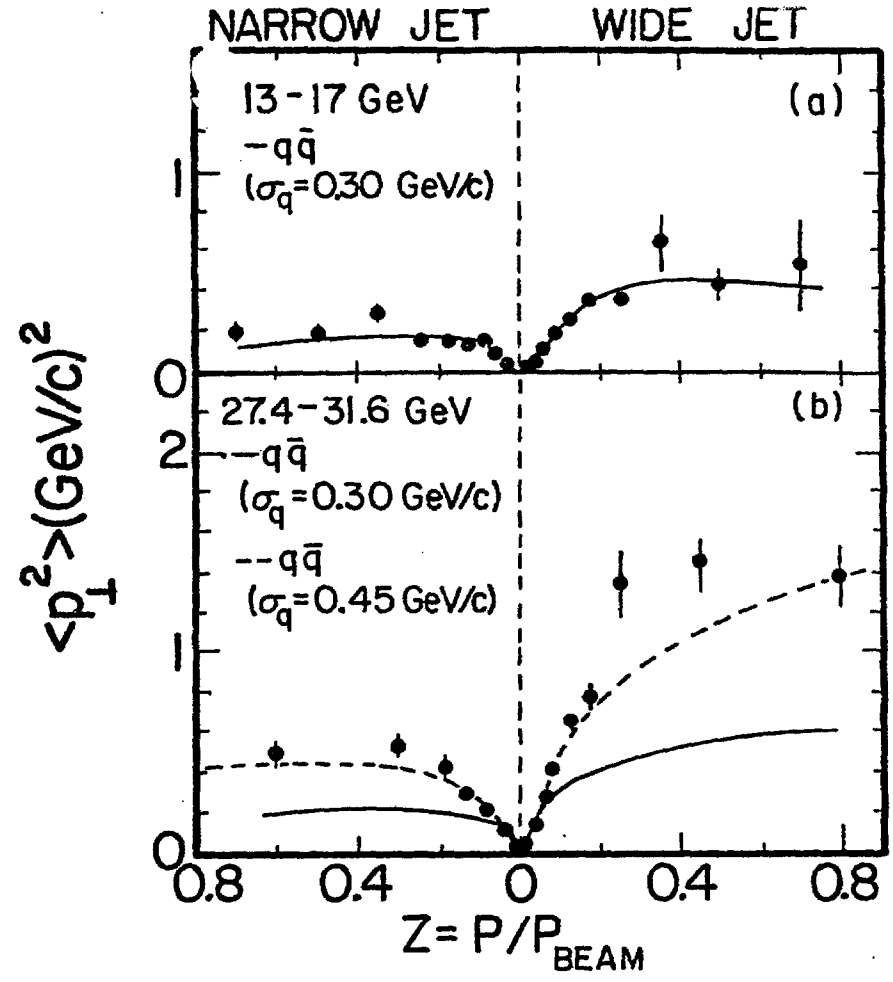
NARROW JET
WIDE JET
13-17 GeV
(a)
$-q\bar{q}$
(σ_q=0.30 GeV/c)
27.4-31.6 GeV
(b)
$-q\bar{q}$
(σ_q=0.30 GeV/c)
$--q\bar{q}$
(σ_q=0.45 GeV/c)
$\langle p_\perp^2 \rangle (GeV/c)^2$
$Z = P/P_{BEAM}$

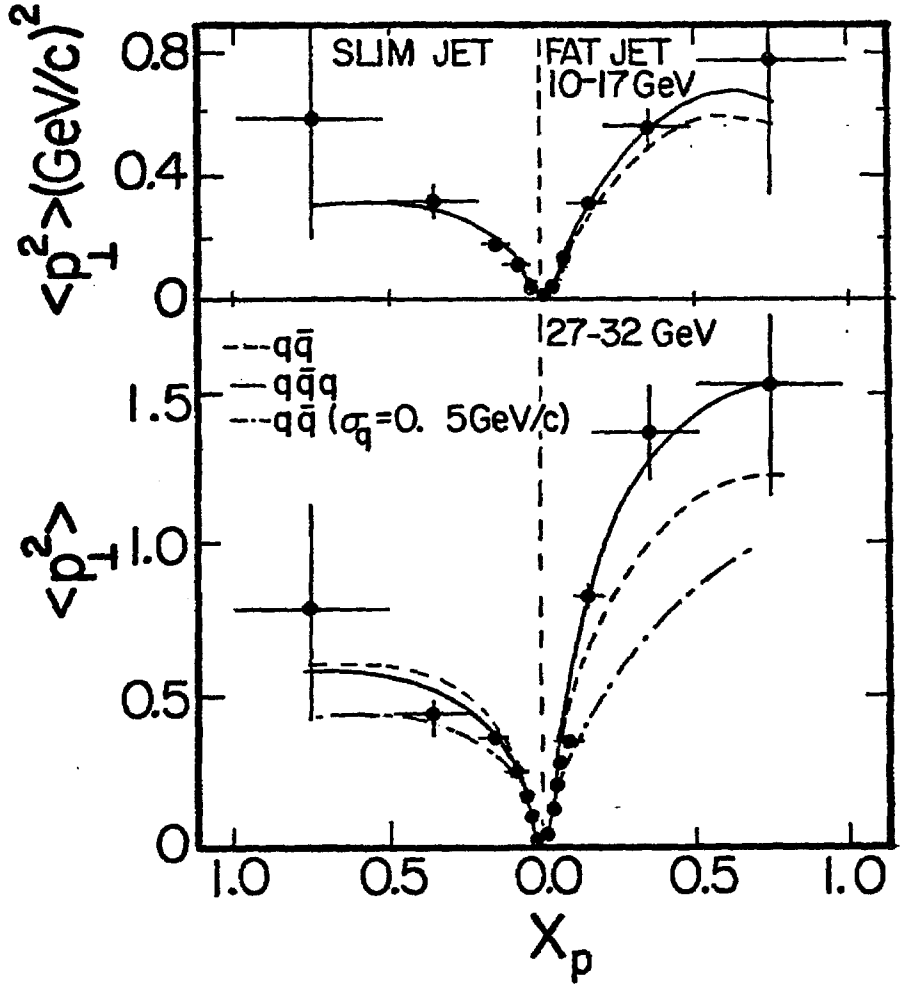
SLIM JET
FAT JET
10-17 GeV
27-32 GeV
$---q\bar{q}$
$-q\bar{q}q$
$-\cdot-q\bar{q}$ (σ_q=0. 5GeV/c)
$\langle p_\perp^2 \rangle (GeV/c)^2$
$\langle p_\perp^2 \rangle$
X_p

Figure 4

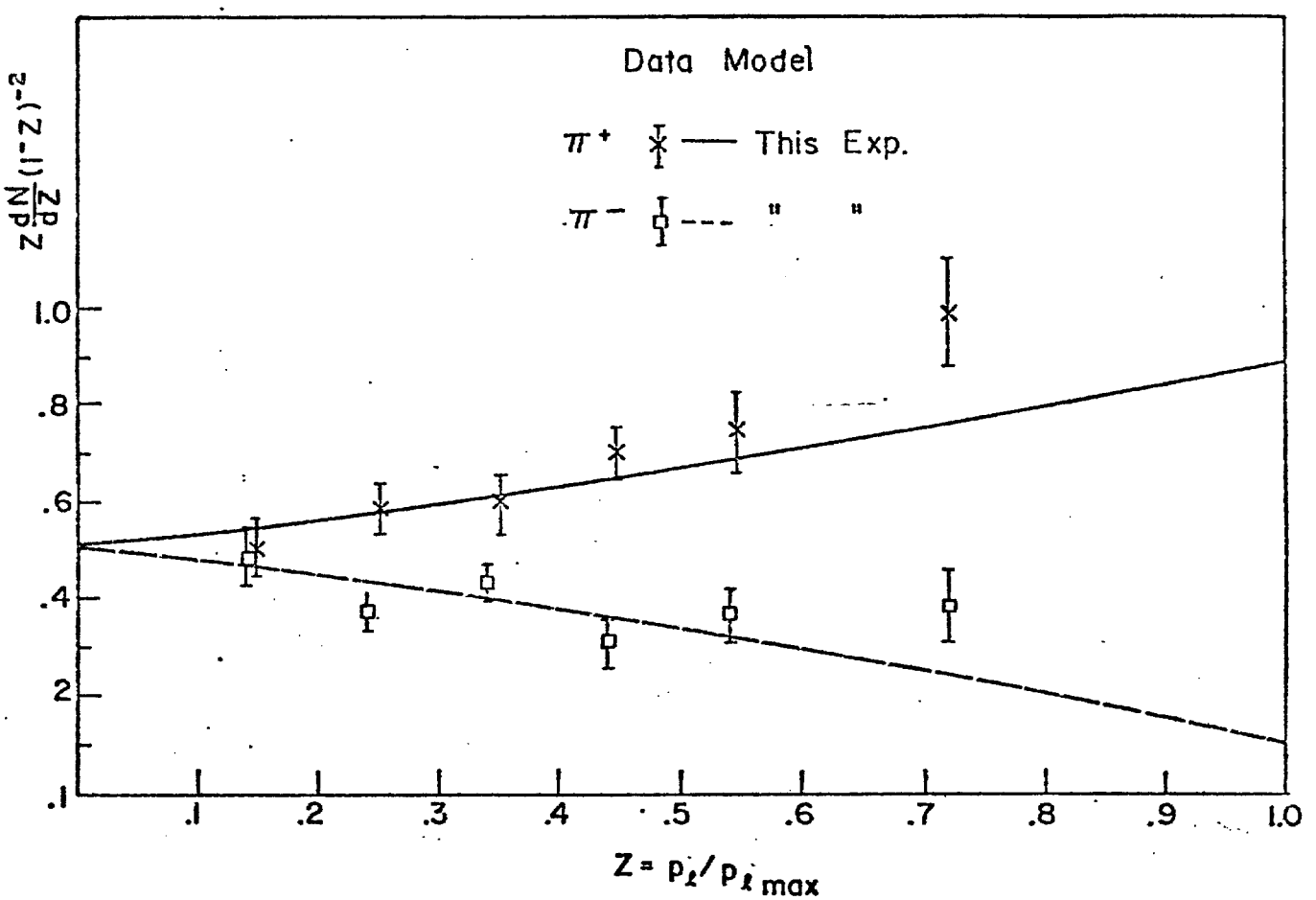

Figure 5 (Ref.8)

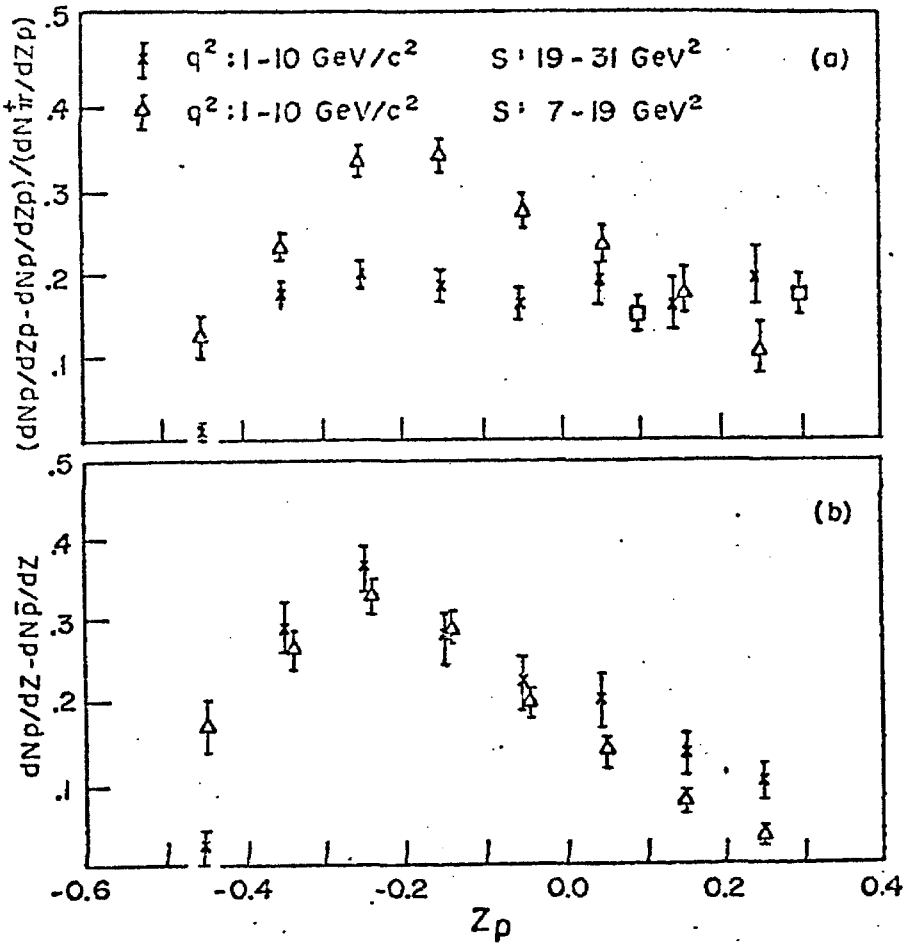

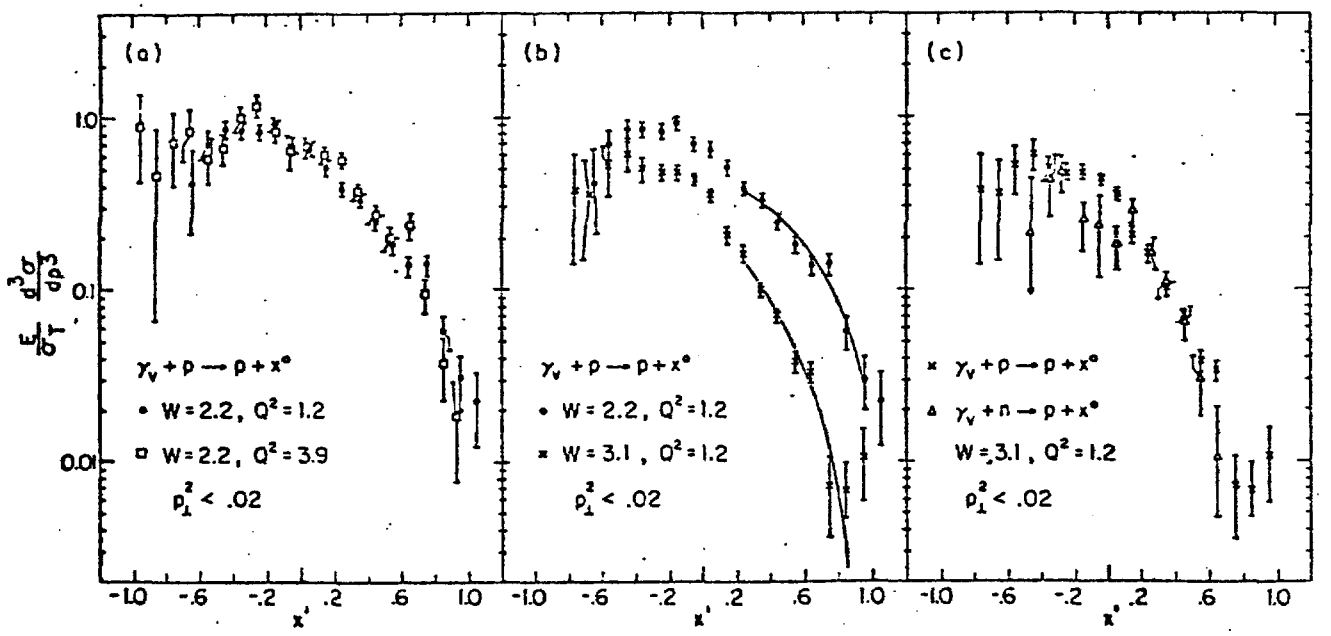

Figure 6 (Ref.12)

ORDER OF MAGNITUDE OF DISTANCE IN
LAB OVER WHICH QUARK FRAGMENTS INTO HADRONS

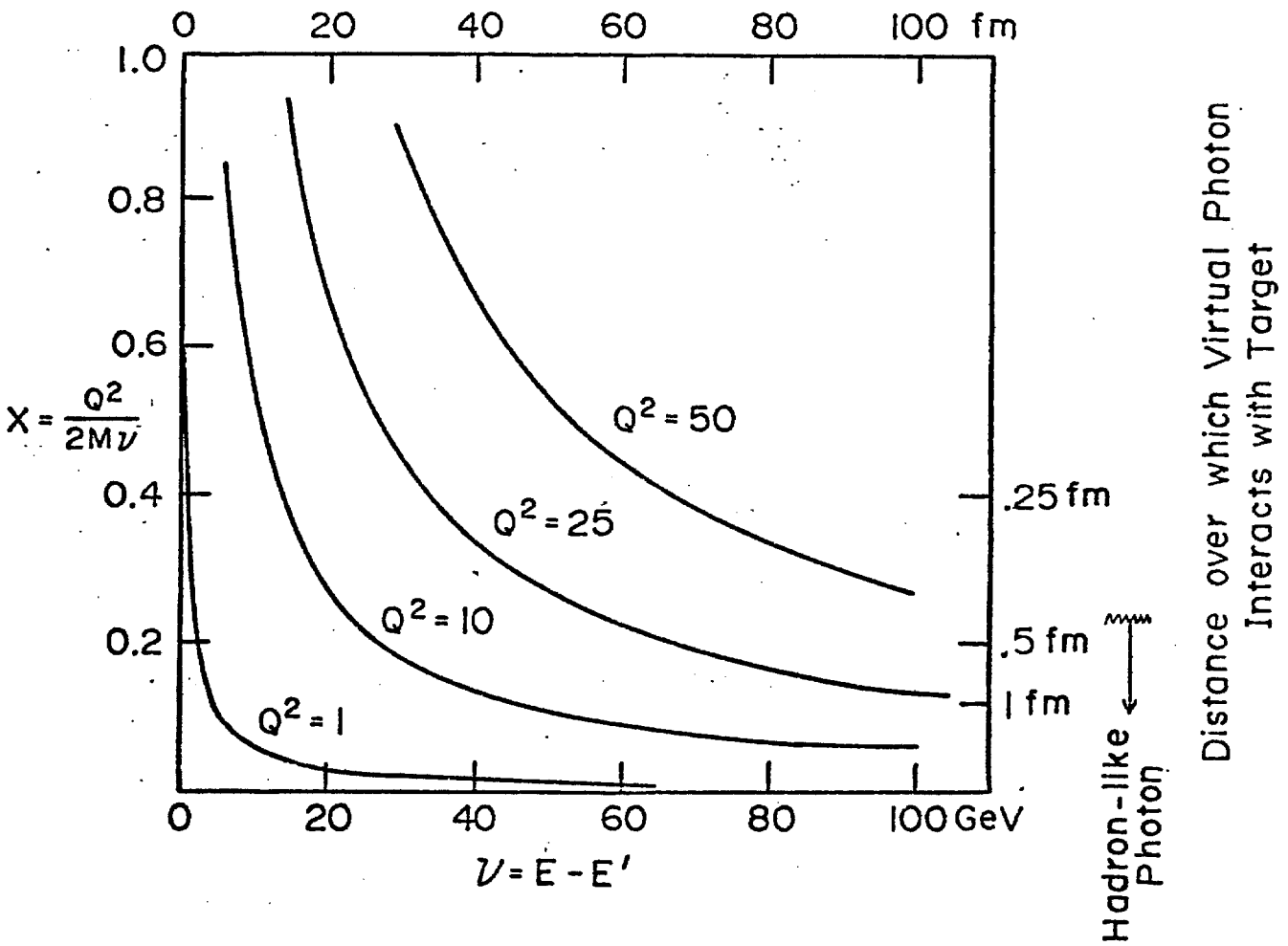

Figure 7

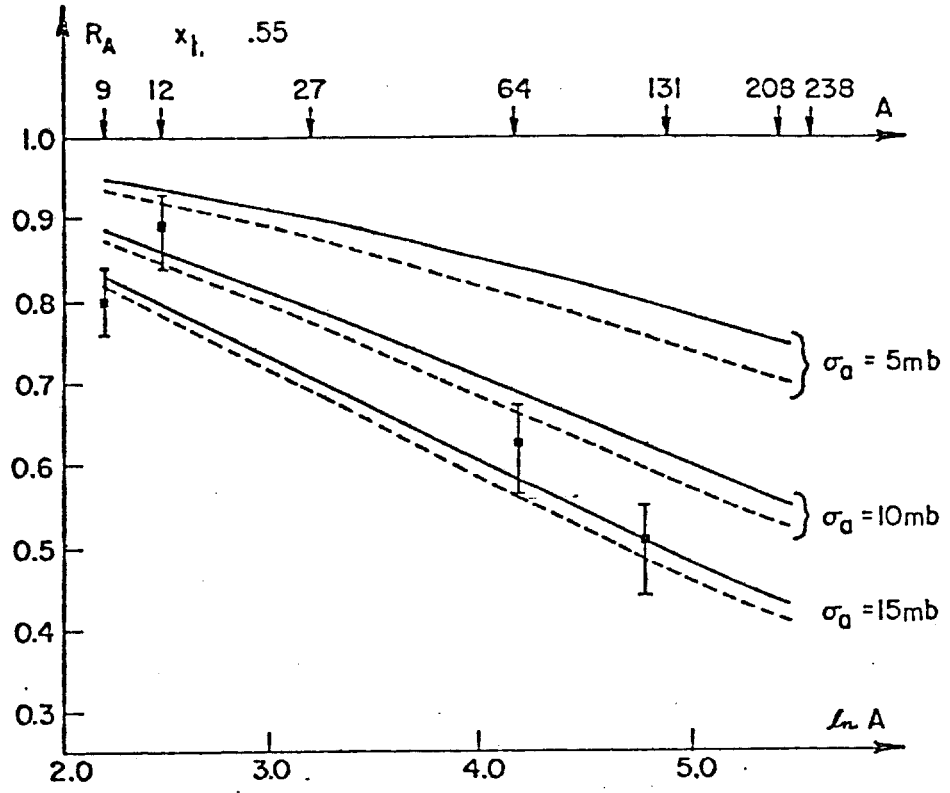

Figure 8 (Ref. 17)

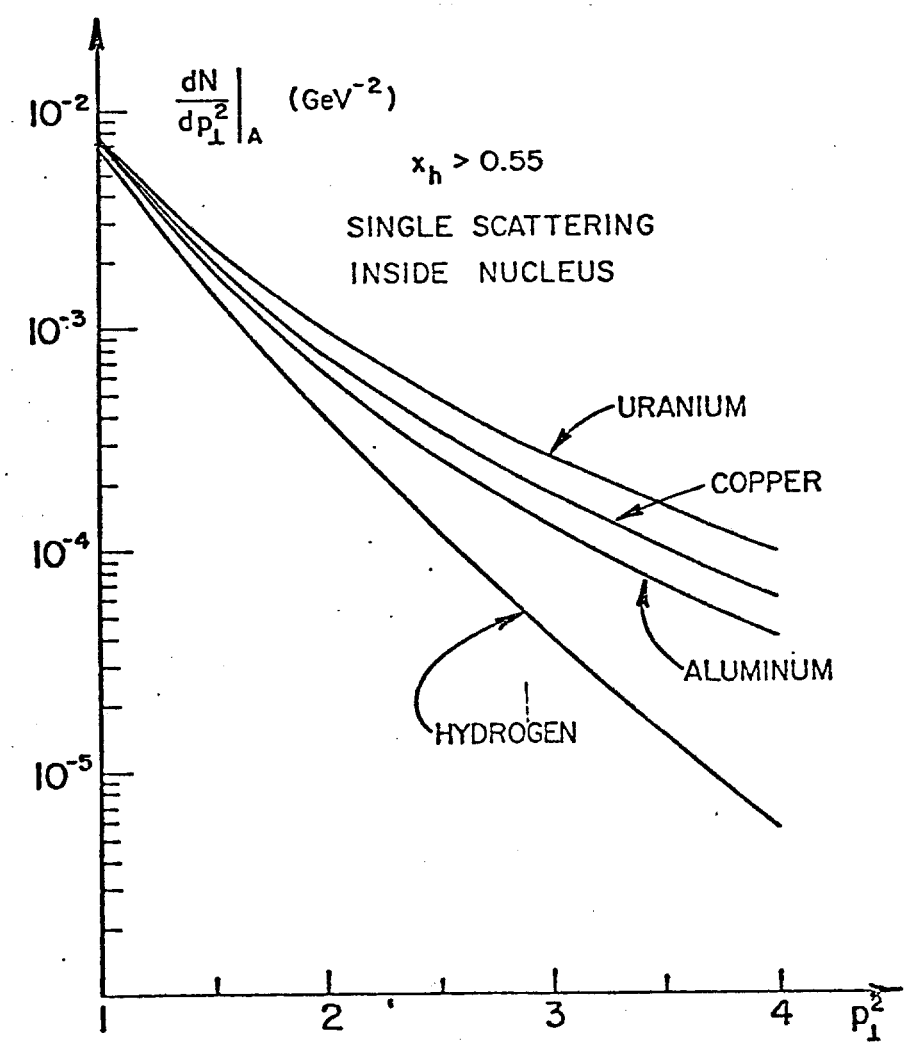

Figure 9 (Ref. 17)

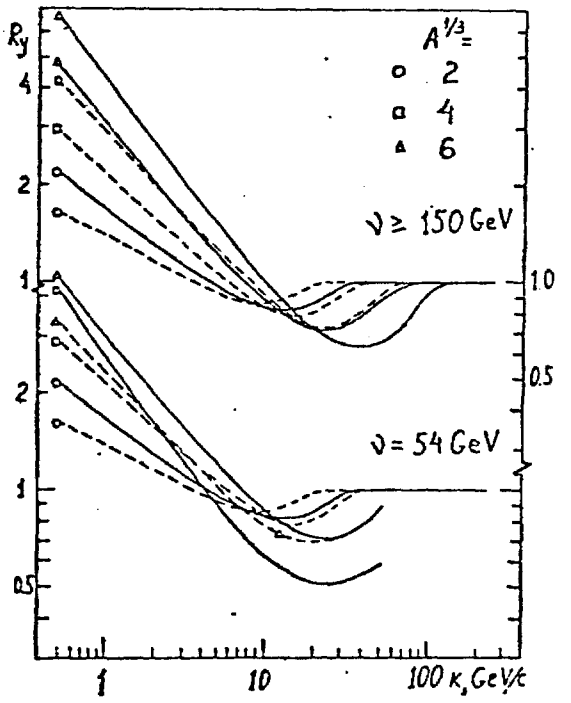

Figure 10 (Ref .18)

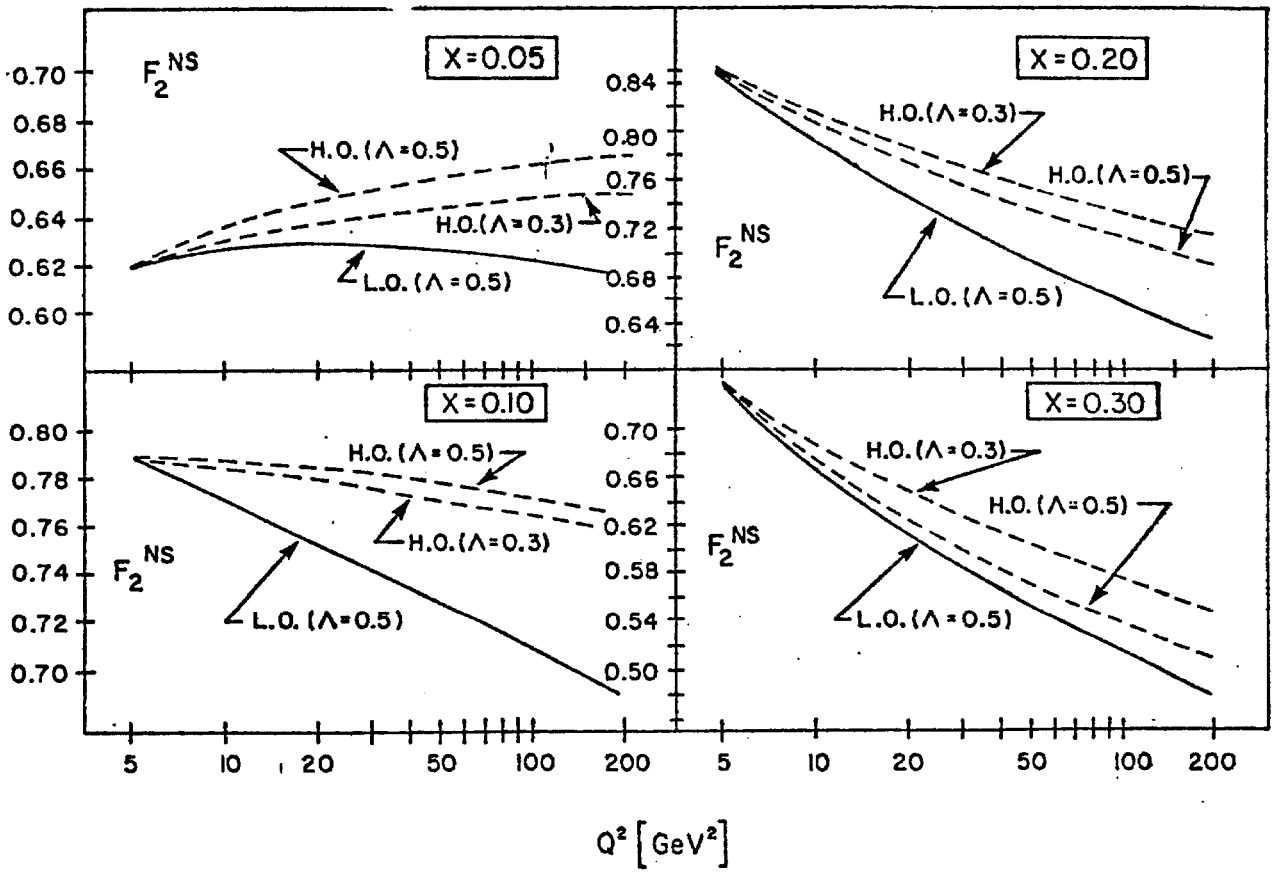

Figure 11a

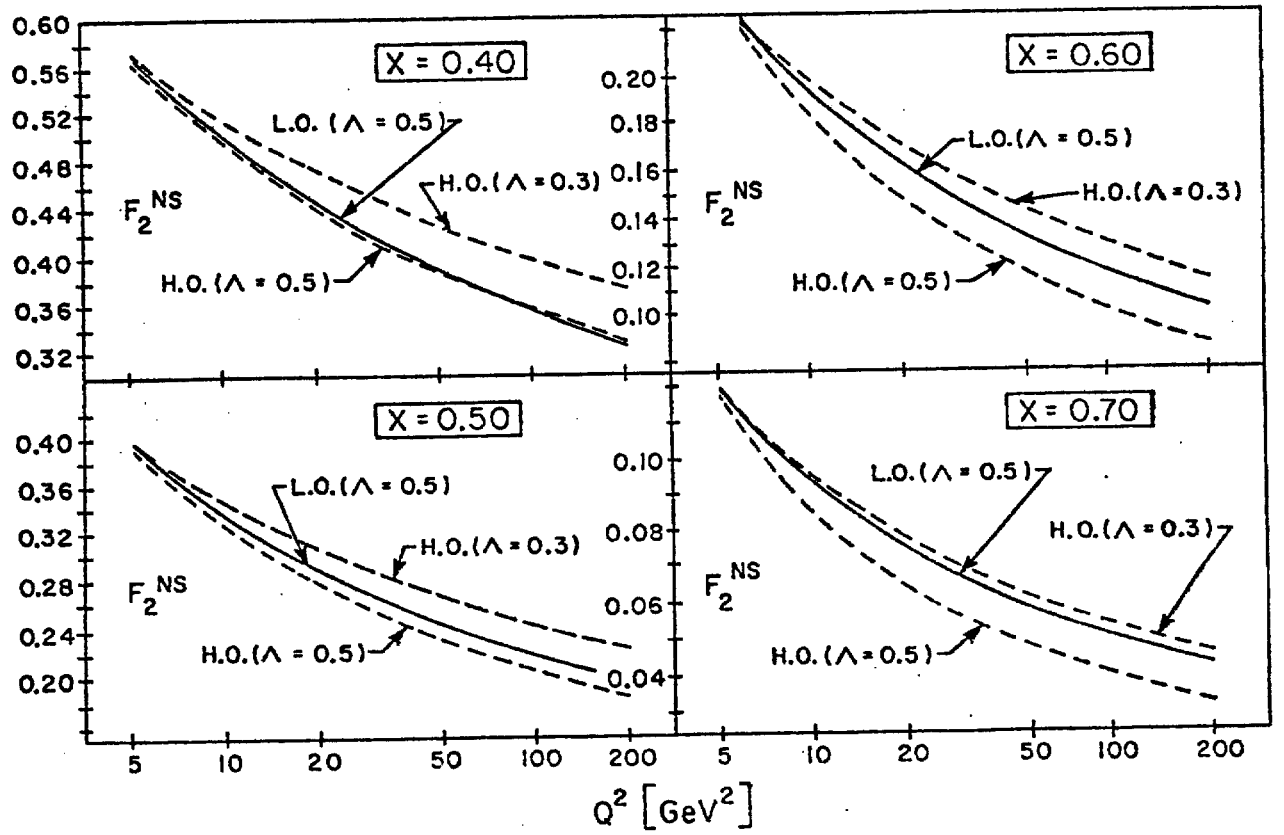

Figure 11b

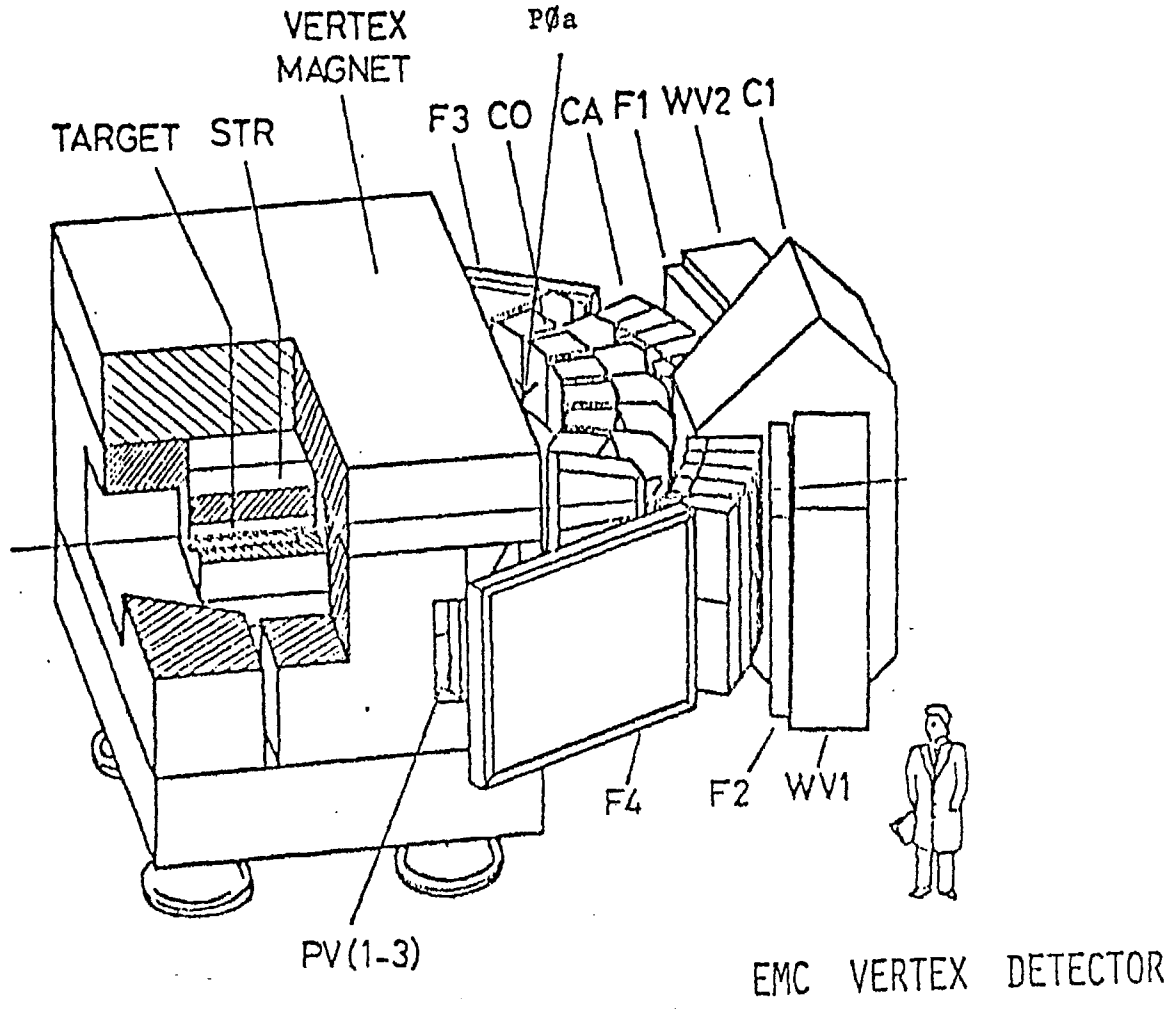
VERTEX
MAGNET
PØa
TARGET
STR
F3
CO
CA
F1
WV2
C1
F4
F2
WV1
PV(1-3)
EMC VERTEX DETECTOR

Figure 12

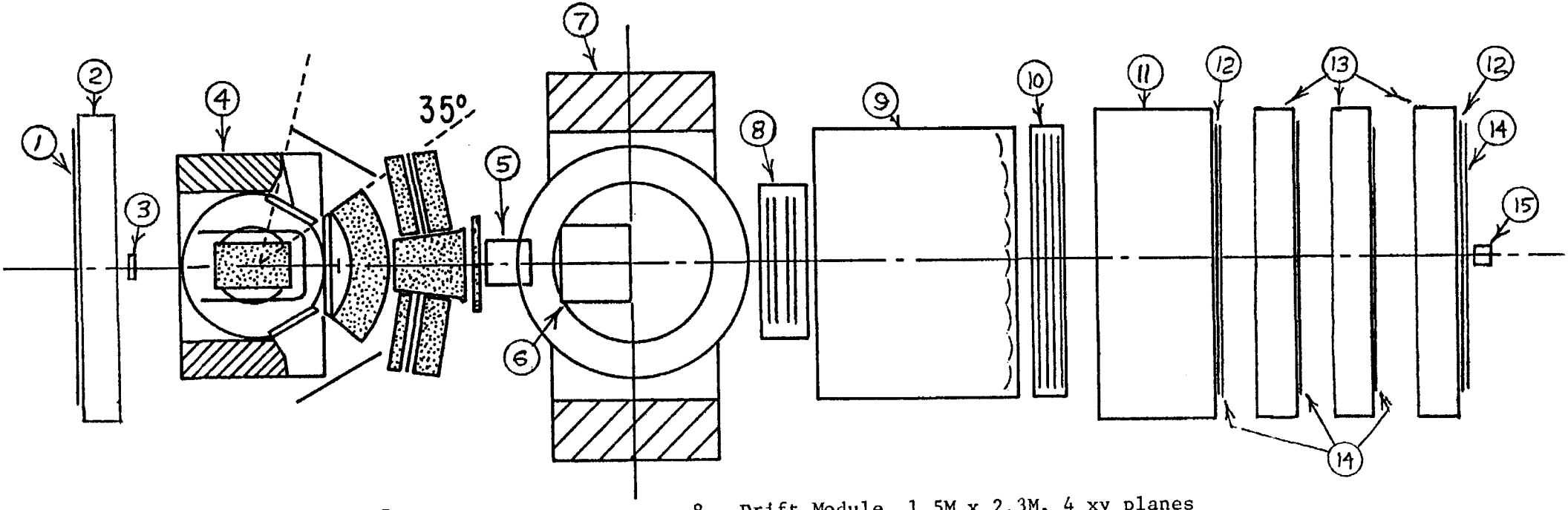

1. Front Veto Wall 4.5M x 7M
2. Backscatter Absorber 5M x 8M
3. Beam Tagging Station, Scin. + MWPC
4. Vertex Spectrometer (Fig. 12)
5. MWPC Module, .8M x .8M, 10 planes
6. MWPC Module, 1.2M x 2.0M, 15 planes
7. Superconducting CCM, 7.5 Tesla M
8. Drift Module, 1.5M x 2.3M, 4 xy planes
9. Cerenkov Counter, 18 cells
10. Drift Module, 4.0M x 7.0M, 6 planes
11. Fe Hadron Absorber, 5M x 8M x 3M
12. M1, M2 Muon Scin. Counters, 4.4M x 7.0M
13. Concrete Absorbers, 5M x 8M x 1M
14. Proportional Tube Planes, 4.4M x 7M, 6 planes
15. Beam Veto Counter

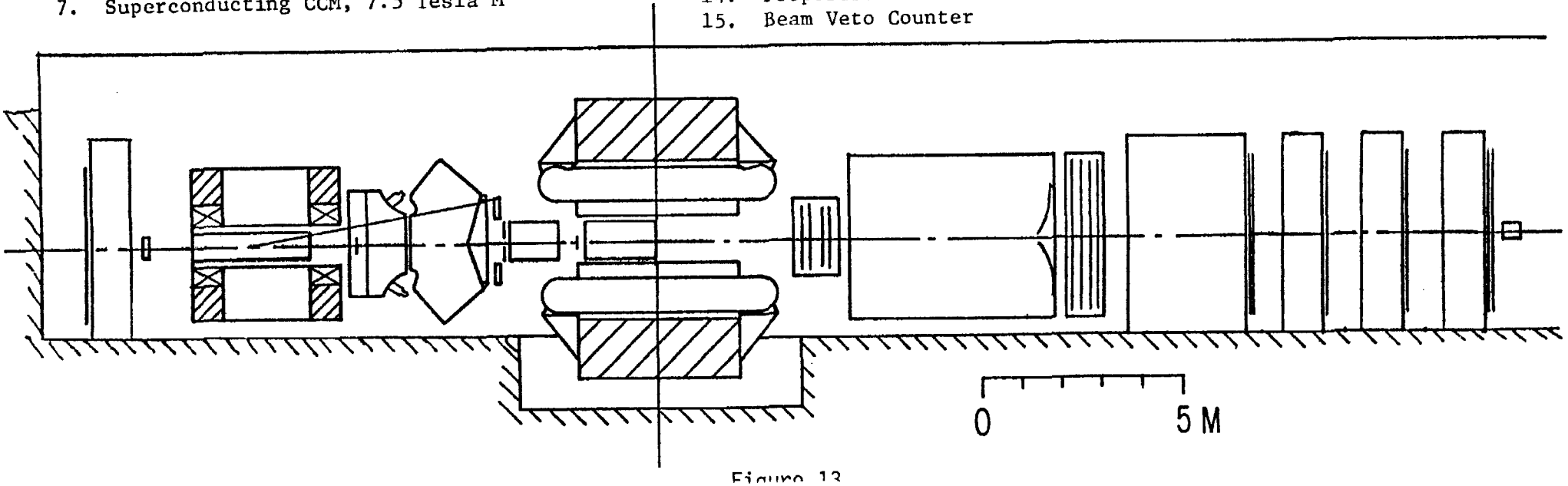

Figure 13

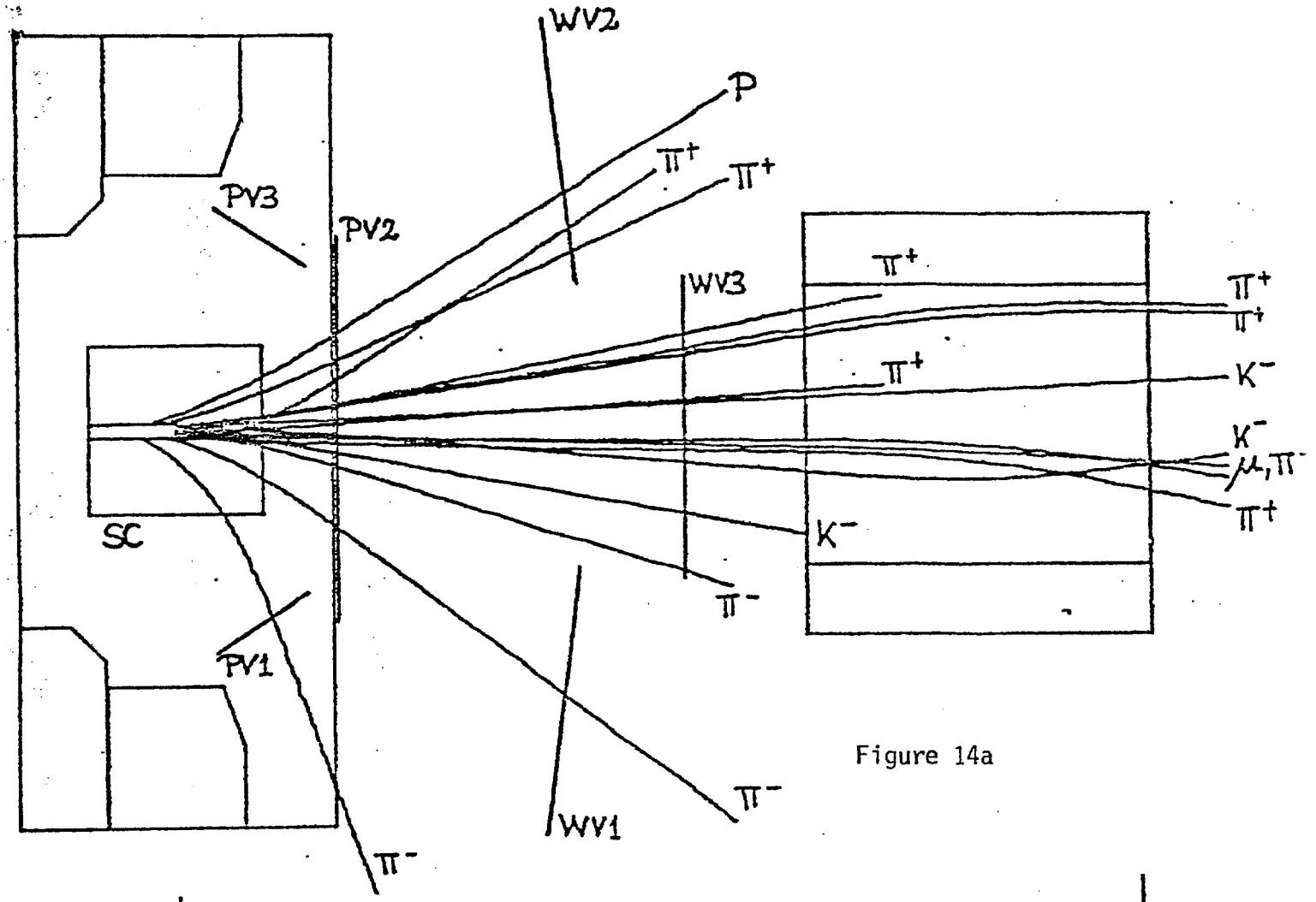

Figure 14a

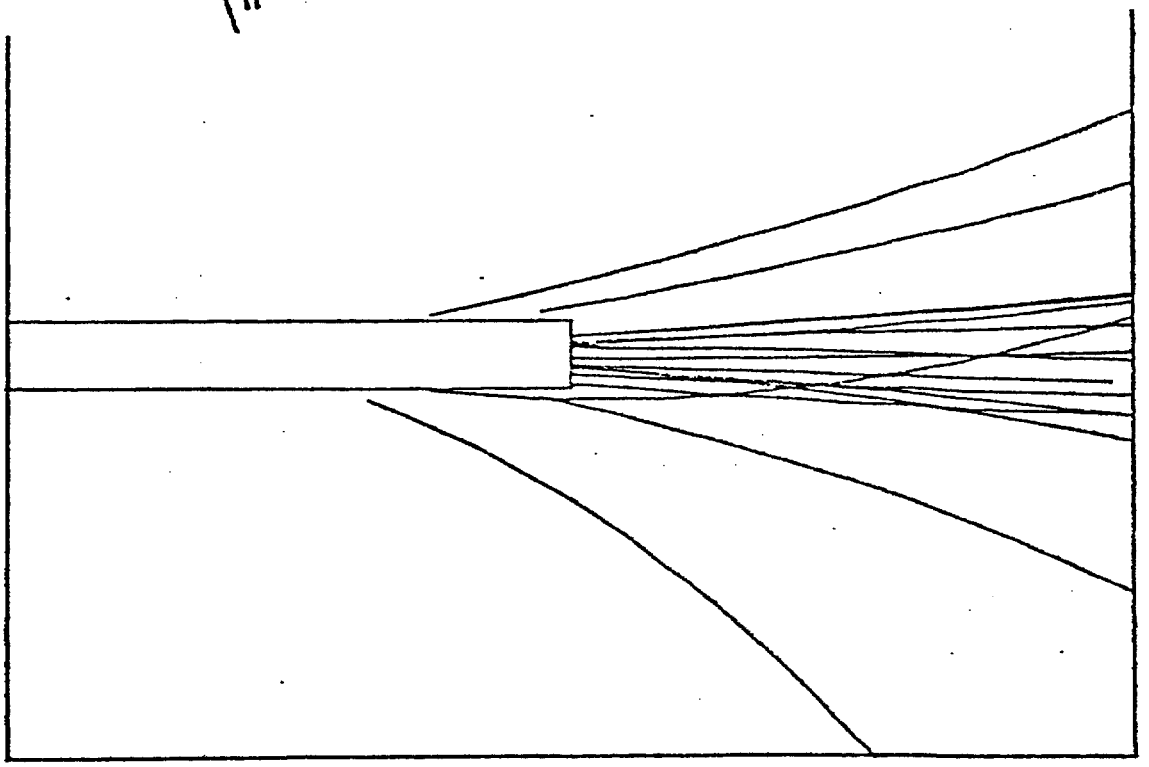

Figure 14b

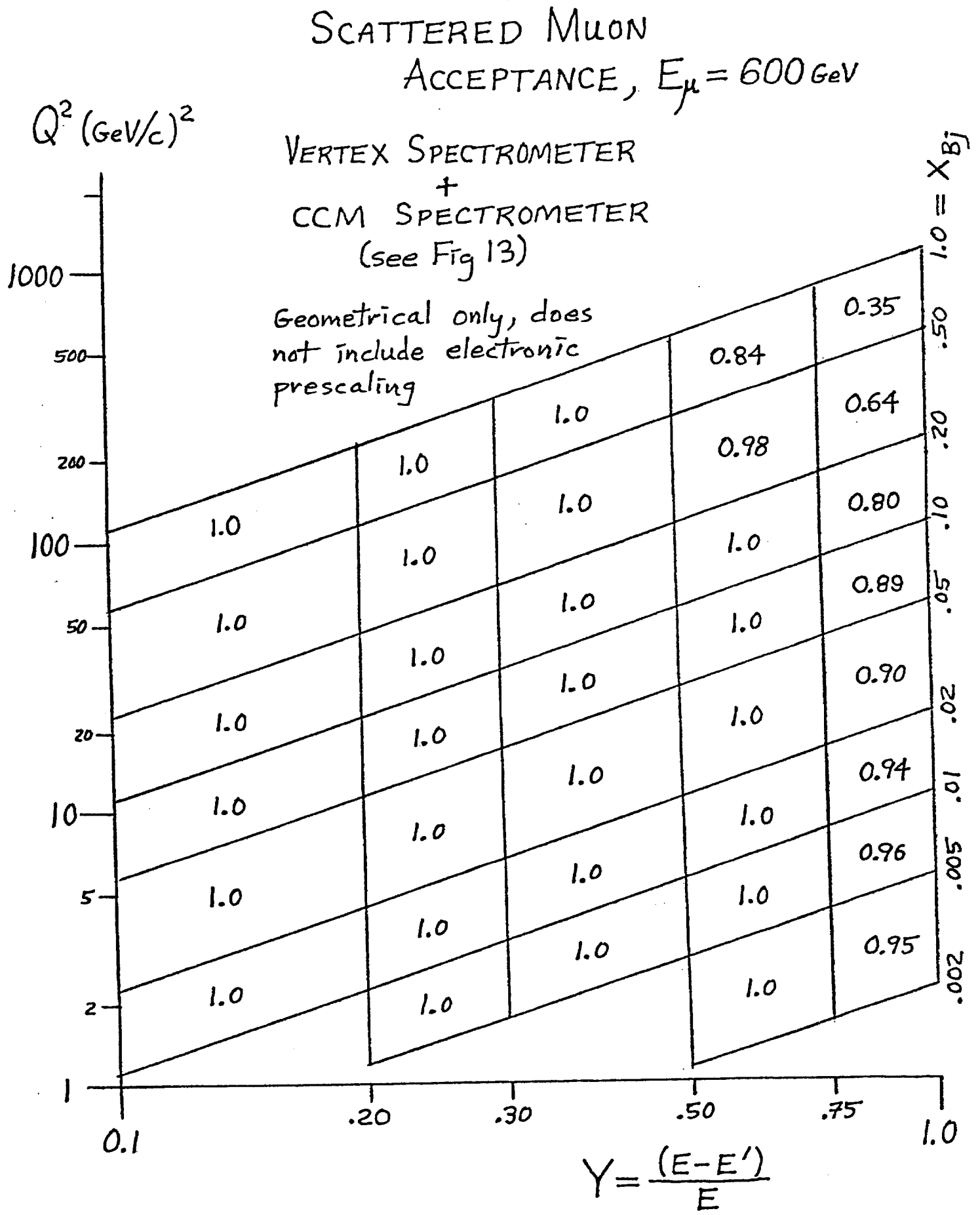
SCATTERED MUON
ACCEPTANCE, $E_\mu = 600$ GeV
VERTEX SPECTROMETER
+
CCM SPECTROMETER
(see Fig 13)
Geometrical only, does not include electronic prescaling
Q^2 (GeV/c)^2
1000
500
200
100
50
20
10
5
2
1
0.1
.20
.30
.50
.75
1.0
$Y = \frac{(E-E')}{E}$
X_{Bj}
1.0
.50
.20
.10
.05
.02
.01
.005
.002
1.0 1.0 1.0 0.84 0.35
1.0 1.0 1.0 0.98 0.64
1.0 1.0 1.0 1.0 0.80
1.0 1.0 1.0 1.0 0.89
1.0 1.0 1.0 1.0 0.90
1.0 1.0 1.0 1.0 0.94
1.0 1.0 1.0 1.0 0.96
1.0 1.0 1.0 1.0 0.95

Figure 15

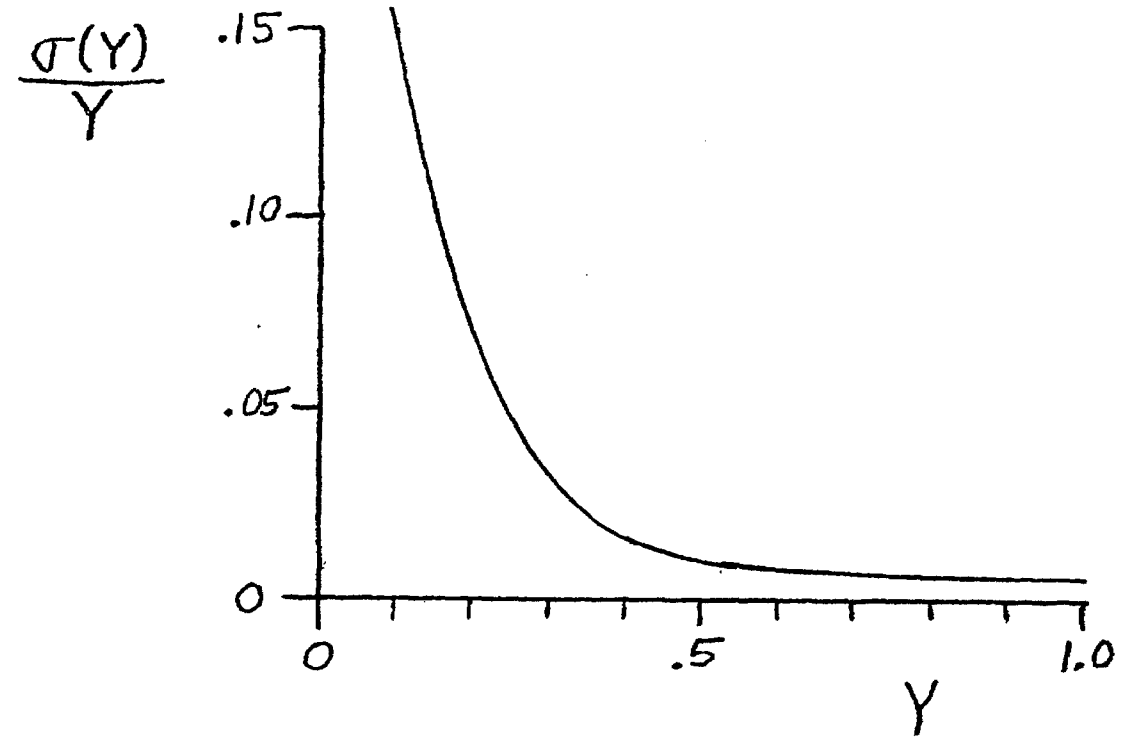

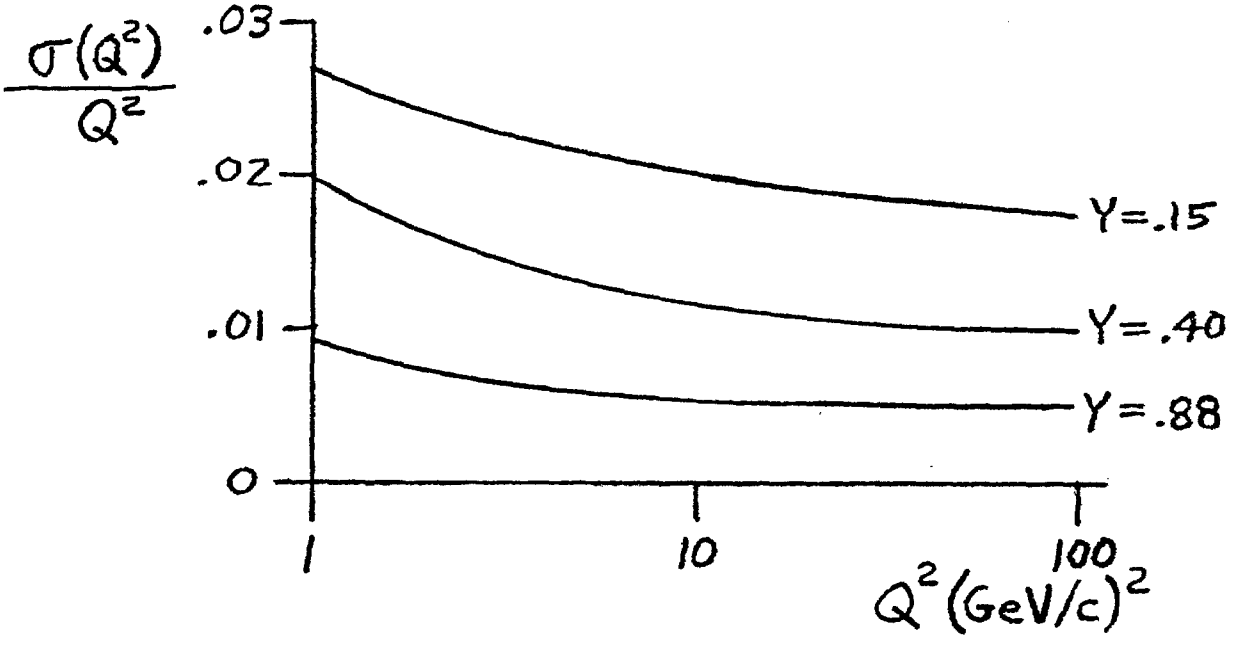

Figure 16

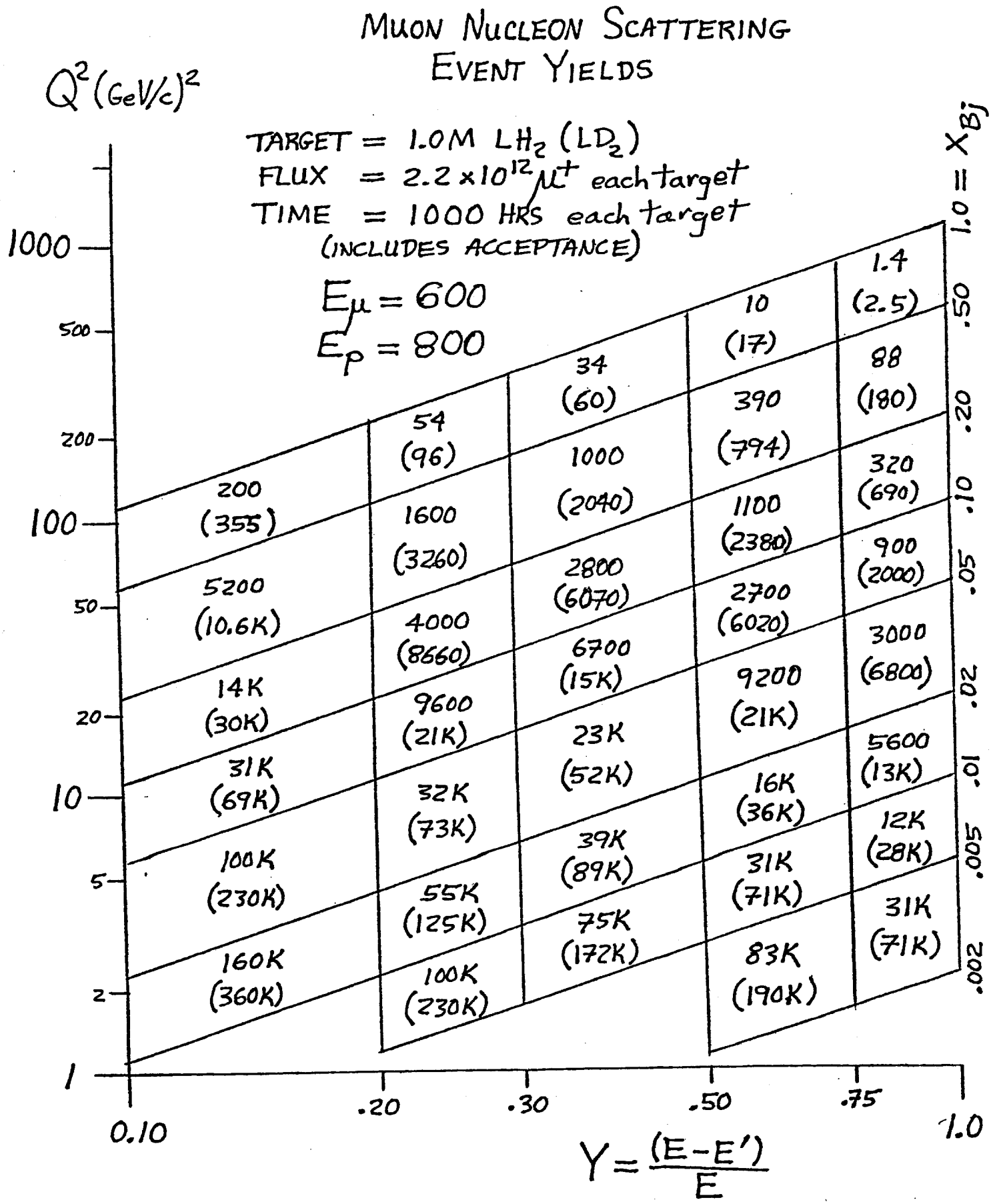
MUON NUCLEON SCATTERING
EVENT YIELDS
Q^2 (GeV/c)^2
TARGET = 1.0M LH_2 (LD_2)
FLUX = 2.2×10^{12} μ^+ each target
TIME = 1000 HRS each target
(INCLUDES ACCEPTANCE)
$E_\mu = 600$
$E_p = 800$
1000
500
200
100
50
20
10
5
2
1
200 (355)
54 (96)
34 (60)
10 (17)
1.4 (2.5)
5200 (10.6K)
1600 (3260)
1000 (2040)
390 (794)
88 (180)
14K (30K)
4000 (8660)
2800 (6070)
1100 (2380)
320 (690)
31K (69K)
9600 (21K)
6700 (15K)
2700 (6020)
900 (2000)
100K (230K)
32K (73K)
23K (52K)
9200 (21K)
3000 (6800)
160K (360K)
55K (125K)
39K (89K)
16K (36K)
5600 (13K)
100K (230K)
75K (172K)
31K (71K)
12K (28K)
83K (190K)
31K (71K)
$1.0 = X_{Bj}$
.50
.20
.10
.05
.02
.01
.005
.002
0.10
.20
.30
.50
.75
1.0
$Y = \frac{(E-E')}{E}$

Figure 17

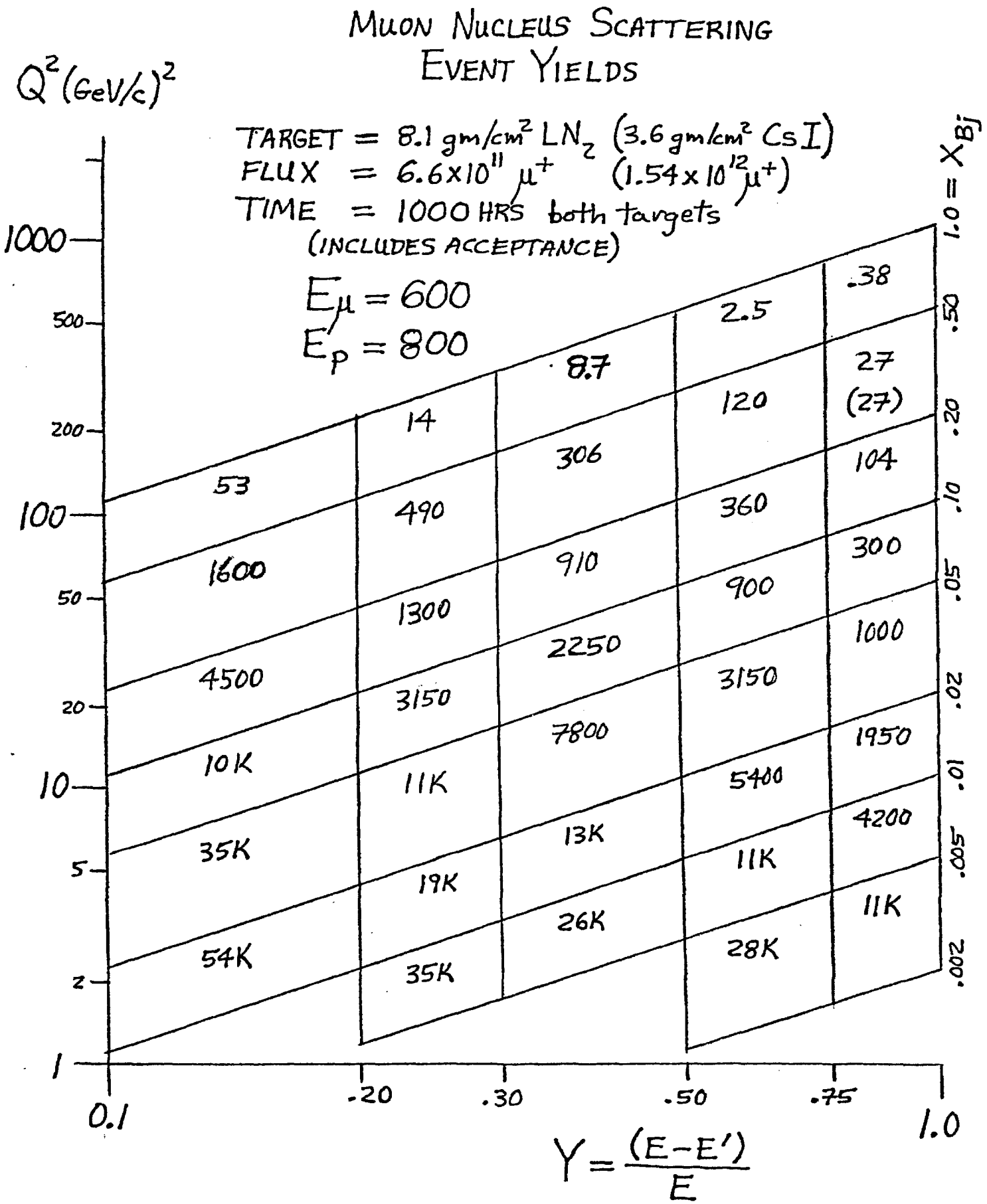
MUON NUCLEUS SCATTERING
EVENT YIELDS
$Q^2 (GeV/c)^2$
TARGET = 8.1 gm/cm² LN_2 (3.6 gm/cm² CsI)
FLUX = 6.6x10¹¹ μ⁺ (1.54x10¹² μ⁺)
TIME = 1000 HRS both targets
(INCLUDES ACCEPTANCE)
$E_\mu = 600$
$E_p = 800$
1000
500
200
100
50
20
10
5
2
1
53
14
8.7
2.5
.38
1600
490
306
120
27
(27)
4500
1300
910
360
104
10K
3150
2250
900
300
35K
11K
7800
3150
1000
54K
19K
13K
5400
1950
35K
26K
11K
4200
28K
11K
0.1
.20
.30
.50
.75
1.0
$Y = \frac{(E-E')}{E}$
$1.0 = X_{Bj}$
.50
.20
.10
.05
.02
.01
.005
.002

Figure 18

APPENDIX A

Muon Trigger Hardware

The elements of the scattered muon trigger module are shown in Fig. A.1. This module also appears in Fig. 13 in less detail but showing more clearly its relationship to the entire spectrometer. The elements of the muon trigger are:

i) a clearly defined beam muon incident on the target (CB).

ii) a small beam veto counter centered on the unscattered beam and located downstream of the muon module (VB).

iii) two large, approximately segmented trigger planes of scintillation counters, each approximately 4.4M x 7.0M in size (M1, M2)

iv) a set of 6 proportional tube planes distributed as shown in Fig. A.1 separated by concrete absorbers and subtending the same solid angle as the scintillation planes (T1 - T6)

v) a large scintillation counter front veto wall of size which suppresses halo muon initiated triggers (V).

We discuss these in some detail in this appendix prior to explaining how they are used in Appendix B.

The CB signal comes from a set of 6 beam scintillation hodoscopes, each containing 6 counter elements of 1.8cm width and 12cm length. These hodoscopes are placed as follows: BH1 immediately downstream of the final beam quadrupole; BH2 just upstream of the momentum tagging dipole; BH3, BH4 just downstream of the tagging dipole; BH5, BH6 just upstream of the vertex magnet spectrometer. BH3, BH5 have horizontal counter elements (y-measuring). All the rest have vertical elements (x-measuring). In combination, the beam hodoscopes define a muon which is in the beam and crudely specify its momentum and incoming trajectory to the target.

Around the tagging dipole physical aperture are placed veto counters which delineate the aperture electronically and veto any beam muon that has scraped the sides of the tagging dipole in passing through it.

Many of the counters needed to implement CB exist at present, although the tagging counter hodoscope elements may need to be resized slightly to satisfy the new conditions. The veto aperture counters and beam veto exist.

The detailed geometry of the trigger planes M1 and M2 has not been worked out yet, but the general features of the elements are already clear. There will be of order 50 counters in each plane. Since each array is about $30M^2$ in size, this means an individual counter will be about $0.6M^2$ in area. Counters near the beam always have higher singles rates and will be smaller. Counters far from the beam have lower rates and can be larger. Linear dimensions will be held to 1.0M or less to allow resolution times within a single rf bucket of the accelerator (18 ns period).

The proportional tube planes will be fabricated from extruded aluminum shapes. Each extrusion will define two half overlapped planes of spacing 2.5cm. This geometry gives both good efficiency and adequate resolution for a fast determination (~ 50-100μs) of the scattered muon trajectory by a microprocessor based trigger processor. As shown in Fig. A.1, there are six of these dual proportional tube planes arranged as xy, x, y, xy. The individual planes are decoupled by concrete absorbers to minimize the influence on the pattern recognition of soft showers which routinely accompany muons emerging from thick absorbers.

In front of the M1 plane is a large Fe absorber which removes all the hadrons from the trigger by nuclear absorption. Muons from hadron decay in flight in the spectrometer together with prompt muons from nuclear interactions of the secondaries in the Fe absorber cause the scattered

muon be accompanied by a second or third muon in a few percent of the events. From experience, we know that the true scattered muon can be identified in almost every case. The data must be corrected for the small remaining sample of ambiguous multimuon events.

The large veto wall in front of the apparatus exists at Fermilab and has been used successfully in a number of experiments already. Its purpose is to veto halo muons which move through the dirt outside the beam region. These muons can simulate real muon scatters when combined in accidental coincidence with a beam muon that does not count in VB. The halo veto suppresses these triggers.

There are presently about 24 counters in the veto wall. They are about 1.5M x .6M in size and can be brought into 1 rf bucket time resolution if desired. When halo single rates are low, however, the veto wall is often stretched to cover 2 rf buckets for safety.

The electronic means for latching and reading in the muon trigger counters and prop tubes is not yet finalized, nor is the exact design of the trigger processor. Clearly there are precedents for both and we view the decisions to be made in the vein of <u>which</u> scheme to use, not <u>whether</u> any scheme will work. The counters and tubes will be recorded at 1 bit per channel, a circumstance which is covered in many existing input registers for costs of order $20/wire. At this rate, the input system, exclusive of the microprocessor pattern unit should cost on the order of $20 x 3000 channels = $60K. The processor unit should have a comparable cost.

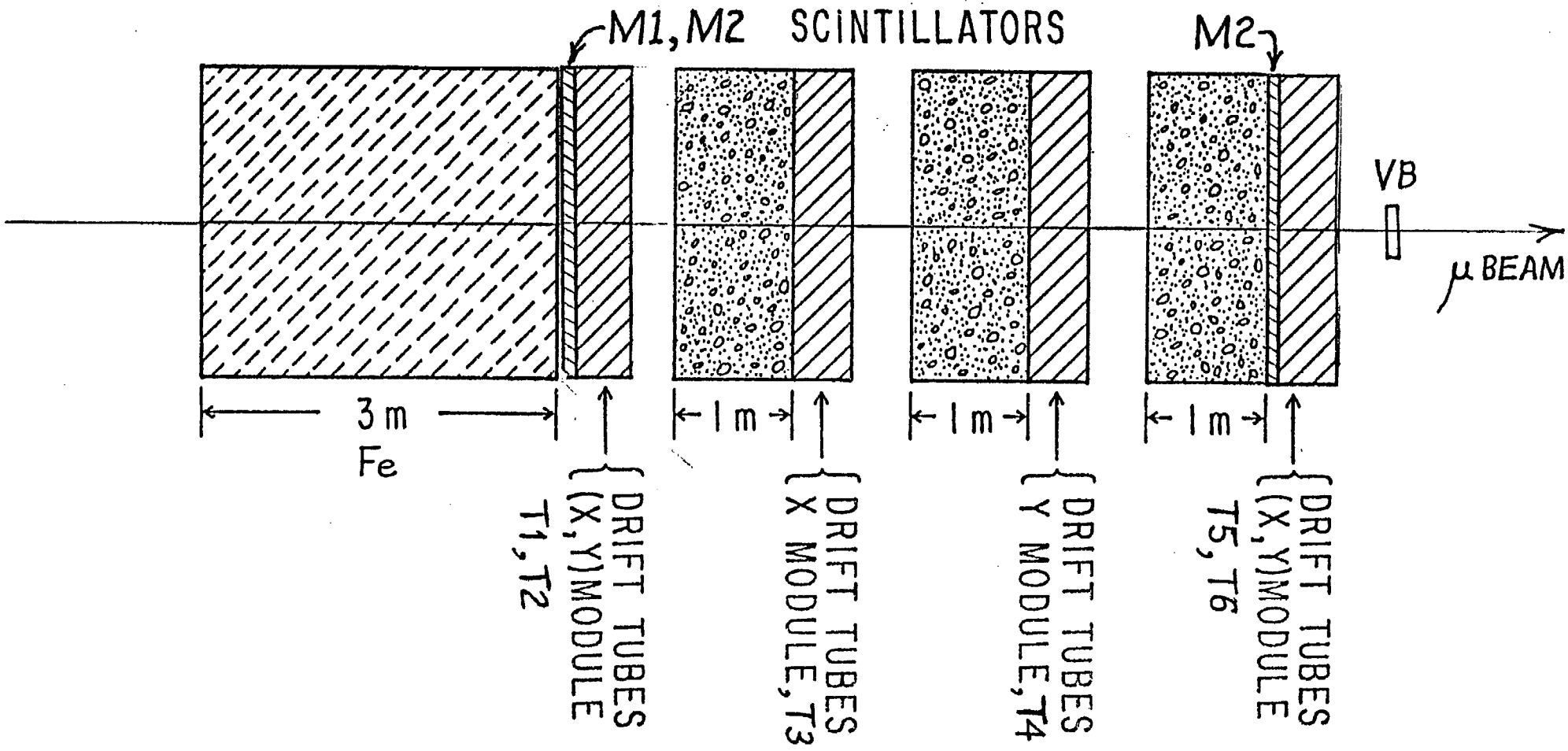

DETAIL OF MUON DETECTOR (SCHEMATIC)

Fig. A.1

APPENDIX B

Trigger Logic

The hardware described in Appendix A is used to trigger on muons scattered by the target located in the vertex spectrometer and to suppress triggers from all other sources. The equal angle focussing principle discussed in Appendix C is used in an approximate way to aid the trigger prescaling scheme which we discuss below. A fast/slow system is used in which scintillation planes M1 and M2 first detect muons scattered out of the beam and then proportional tubes select the good muon scatters on the basis of pattern recognition by a microprocessor based event selector. Special triggers are used for diagnostic purposes. We cover the details here.

The fast trigger for the apparatus is given by:

$$T_i = CB \cdot \overline{VB} \cdot (M1 \cdot M2)_i \cdot \overline{V},$$

where;

T_i = ith fast scattered muon trigger; these triggers will be prescaled to balance statistics

M1, M2 = Scattered muon scintillation hodoscopes; various combinations of M1 and M2 elements are combined to make the ith prescaled fast trigger.

VB = beam centered veto counter behind the scattered muon planes

V = veto wall in front of the vertex spectrometer (approx. 7M x 4M)

CB = cleanly transmitted muon beam particle

CB = $BH1 \cdot BH2 \cdot (BH3 + BH4) \cdot (BH5 + BH6) \cdot \overline{VA}$

BH_j = jth beam hodoscope (OR of 6 counters in each plane)

VA = veto counters around tagging dipole apertures

The CB part of the trigger insures a beam muon cleanly transmitted to the target. The veto wall discriminates against halo particles moving roughly parallel to the beam which constitute a prime source of accidental coincidence triggers. The various $(M1 \cdot M2)_i$ combinations give scattered muon

coincidence triggers. Since very low Q^2 triggers can arise from a variety of sources, the principal one being μe elastic scatters, the higher rate combinations will be prescaled to give a statistically sufficient sample, but one which does not clog the data processing machinery.

The CB • M1 • M2 coincidence says a beam muon entered the target and a muon passed through the muon module. For a real event, the muon will also be absent from the beam. This is the purpose of the small beam veto count VB. It is used in anticoincidence. The rate for CB • $\overline{VB}$ • $\overline{V}$ is about 5×10^{-5} with contributions from muon decay in flight, interactions in the Fe absorber and the exp. target and VB inefficiency. The (M1 • M2) requirement will drop the CB • $\overline{VB}$ • $\overline{V}$ rate by a factor of 125 after prescaling to yield a raw trigger rate of 0.4×10^{-6}. With our proposed beam of 4×10^7/pulse, this yields 16 triggers/20 sec spill, an easy rate to handle.

These rates are based on our experience, but even if there are "junk" triggers at a level 100 times as great, our trigger processor can sort these out at the rate of 1 trigger/100μs, thus keeping the experimental deadtime below a few percent, i.e.;

$$f_{dead}(\text{fast}) \leqq \left(16 \frac{\text{real trigs}}{\text{pulse}}\right) \left(100 \frac{\text{junk}}{\text{real}}\right) \left(10^{-4} \frac{\text{secs}}{\text{trig}}\right) \left(\frac{1}{20 \text{ secs/pulse}}\right)$$

$$f_{dead}(\text{fast}) \leqq 0.008 \text{ (deadtime fraction from fast triggers)}$$

The event rate for which data is recorded depends upon the tightness of the criteria imposed by the trigger processor on the data presented by the fast trigger;

$$E_i = f(T_i, \text{ prop tubes, scin, etc.}),$$

where;

E_i = accepted event fraction of T_i which is fully recorded

$f(T_i$, prop tubes ....) = microprocessor based pattern recognition for the data in the muon module to accept good scatters and reject junk

If we assume that an appropriate algorithm, passes twice as many fast triggers as eventually become good events, we find:

$$E_i = \left(2 \frac{\text{slow trigs}}{\text{good event}}\right) \left(16 \frac{\text{good events}}{\text{pulse}}\right) = 32 \frac{\text{slow trigs}}{\text{pulse}} .$$

And, if our full data readin time is 10 milliseconds/event, we find the dead time due to slow event triggers is given by:

$$f_{dead}(\text{slow}) = \left(32 \frac{\text{trigs}}{\text{pulse}}\right) \left(10^{-2} \frac{\text{sec}}{\text{trig}}\right) \left(\frac{1}{20 \text{ sec/pulse}}\right)$$

$$f_{dead}(\text{slow}) = 0.014 \text{ (deadtime fraction from slow triggers).}$$

Adding the deadtime fractions for fast and slow triggers together we get;

$$f_{dead}^{(\text{total})} = f_{dead}(\text{fast}) + f_{dead}(\text{slow})$$
$$\leqq 0.022.$$

The deadtime is clearly not a problem.

How about data recording and processing? We will use a 6250 bpi tape recorder for the data acquisition. We expect each event to have about 2000 words of 16 bit data. With the recording speed of these units and a two buffer core system, the data logging to tape easily keeps up with the slow trigger. A 2400 foot recording tape should hold about 5000 slow triggers. A 1000 hour run will generate a total of 1.9×10^6 slow triggers presenting a challenging but not unheard of analysis assignment.

APPENDIX C

Dipole Magnet Focussing

Two dipole magnets can be used to obtain a dispersion free "focus" if their bending fields are of opposite sign and the B field magnitudes are related properly to the distances involved. In the case of the Vertex Spectrometer Magnet and the CCM, an exact focus (neglecting fringe fields and large angle rays) can be made at point B (See Fig. B.1).

The appropriate condition is given by:

$$P\ (CCM) = -\left(\frac{D1 + D2}{D2}\right)\ P\ (VM),$$

where; P = Transverse momentum kick of the dipole $P = \int B dl$.

$D1$, $D2$ = Distances as shown.

The y component of momentum is unchanged in this approximation (paraxial rays).

When the term "focus" is used, it does not mean trajectories of all (paraxial) angles and all momenta leaving point A are imaged to a point at B. What it does mean is that all particles on a given initial trajectory (angles in space) will pass through a common point B, regardless of momentum. Thus, we have what amounts to a "chromatic line to point focus" condition.

The above condition is useful in the proposed spectrometer for two main reasons:

i) it simplifies the prescaling of various fast triggers

ii) it improves acceptance.

In neither case, is it necessary to satisfy the focussing condition exactly. For our geometry, it would mean lowering the CCM current by about 21%, a significant loss in CCM reconstruction resolution.

As a result, we will exploit the advantages of the focussing in a qualitative way without satisfying the exact condition.

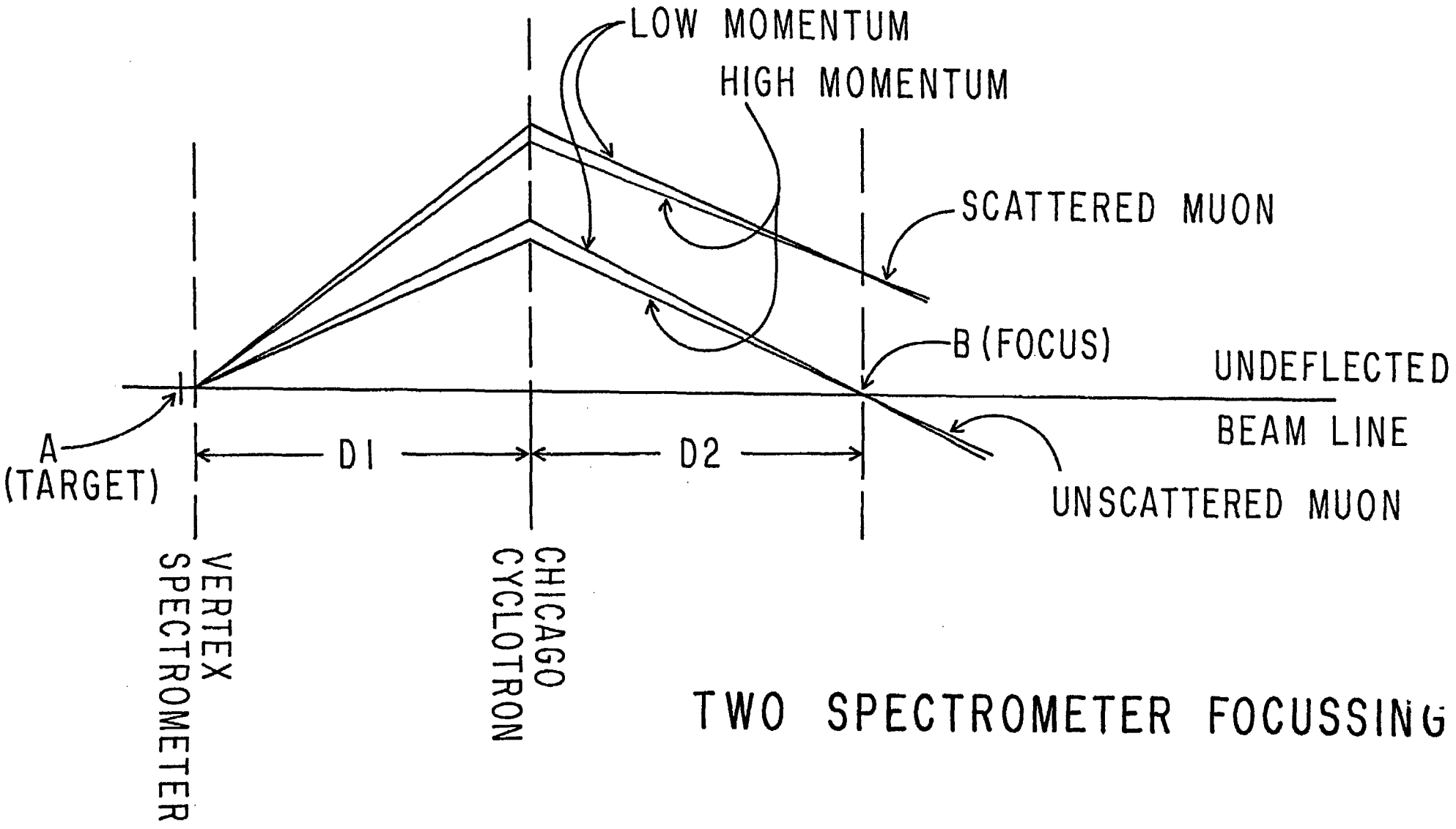
LOW MOMENTUM
HIGH MOMENTUM
SCATTERED MUON
B (FOCUS)
UNDEFLECTED
BEAM LINE
UNSCATTERED MUON
A
(TARGET)
D1
D2
VERTEX
SPECTROMETER
CHICAGO
CYCLOTRON
TWO SPECTROMETER FOCUSSING

Fig. C.1